

# Strong interannual variation of the Indian summer monsoon in the Late Miocene

Hui Tang · Jussi T. Eronen ·  
Arne Micheels · Bodo Ahrens

Received: 15 June 2012 / Accepted: 24 December 2012 / Published online: 30 January 2013  
© Springer-Verlag Berlin Heidelberg 2013

**Abstract** The modern Asian monsoon system exhibits strong interannual variation, which has profound environmental and economical impacts. It has been well-documented that the mean Asian monsoon state underwent significant changes in the Late Miocene (11–5 Ma ago). But how the interannual variability of the monsoon climate evolved during this period is still largely unknown. In this study, a long-term simulation of the Late Miocene with a fully coupled atmosphere–ocean general circulation model (ECHAM5/MPI-OM) at T31L19 resolution is used to explore the interannual variation of the Indian summer monsoon (ISM) in the Late Miocene. The regional climate model COSMO–CLM with a higher spatial resolution ( $\sim 1^\circ \times 1^\circ$ ) is further employed to better characterize the spatial patterns of these variations. Our results show that although the mean ISM circulation is weaker in the Late

Miocene runs, its interannual variation is as strong as or even stronger than at present and the dominant periods ( $\sim 2.6$ – $2.7$  years) are shorter than at present ( $\sim 3.4$ – $8.4$  years). It is noticed that while the extratropical influence on the ISM variability is weaker-than-present, a persistent El Niño–Southern Oscillation with stronger-than-present interannual variability is observed in our Late Miocene run. This may have maintained a strong interannual variation of the ISM with a shorter period in the Late Miocene. Our findings do not only improve our understanding of the Asian monsoon evolution in the Late Miocene, but also shed light on the future changes in the interannual variability of the ISM.

**Keywords** Interannual variability · Indian summer monsoon · ENSO · Late Miocene · AOGCM · Regional climate model

**Electronic supplementary material** The online version of this article (doi:10.1007/s00382-012-1655-y) contains supplementary material, which is available to authorized users.

H. Tang (✉) · J. T. Eronen  
Department of Geosciences and Geography,  
University of Helsinki, P.O. Box 64, 00014 Helsinki, Finland  
e-mail: hui.tang@helsinki.fi

J. T. Eronen · A. Micheels  
Biodiversity and Climate Research Centre (LOEWE BiK-F),  
Senckenberganlage 25, 60325 Frankfurt am Main, Germany

A. Micheels  
Senckenberg Research Institute and Nature Museum,  
Senckenberganlage 25, 60325 Frankfurt am Main, Germany

B. Ahrens  
Institute for Atmospheric and Environmental Sciences,  
Goethe University, Altenhoferallee 1,  
60438 Frankfurt am Main, Germany

## 1 Introduction

The interannual variation of the Asian summer monsoon is a prominent feature of the modern Asian monsoon system (Gadgil 2003; Wang et al. 2001; Webster et al. 1998). The severe droughts and floods caused by such inter-annual behaviour have enormous ecological and social-economic impacts (Cruz et al. 2007; Webster et al. 1998). The presence of the Asian summer monsoon can be traced back to early Cenozoic (Huber and Goldner 2012; Zhang et al. 2012), and a multi-phase development of the mean Asian monsoon climate has been documented by various geological proxies (An et al. 2001; Clift et al. 2008; Sun et al. 2010; Sun and Wang 2005). These developments are primarily attributed to the changes in both global climate and regional tectonics such as the uplift of the Tibetan Plateau

(TP) (An et al. 2001; Dupont-Nivet et al. 2007; Ge et al. 2012; Molnar et al. 2010; Prell and Kutzbach 1992). Among those periods, the Late Miocene (11.6–5.3 Ma) is widely regarded as a crucial period in the Asian monsoon history (Molnar et al. 2010; Quade et al. 1989; Wang et al. 2005; Zachos et al. 2001). A major intensification of the mean state of the Indian summer monsoon (ISM) circulation (Kroon et al. 1991) and the seasonality of precipitation over India (Dettman et al. 2001; Quade et al. 1989; Sanyal et al. 2010) in this period have been inferred from proxy records, which witnessed the emergence of modern ISM climate. Nevertheless, it is still ambiguous how the shift in the mean monsoon climate affected the interannual variability of the ISM during the Late Miocene.

The interannual variation of the ISM is closely linked to atmosphere–ocean interactions. Particularly, it is strongly associated with the El Niño–Southern Oscillation (ENSO) in the tropical Pacific (Gadgil 2003; Ju and Slingo 1995; Wang et al. 2001; Webster et al. 1998). The lighter (heavier) than normal ISM rainfall usually corresponds to positive (negative) phase of ENSO, i.e. the El Niño (La Niña) conditions. Some proxy studies have claimed a permanent El Niño-like condition in the tropical Pacific before the mid-Pliocene (~3–4 Ma ago) (Fedorov et al. 2010; Molnar and Cane 2002; Wara et al. 2005). This may have been responsible for the warmth and the spatial pattern of the mean hydrological changes in these periods (Barreiro et al. 2006; Brierley and Fedorov 2010; Goldner et al. 2011; Shukla et al. 2009; Vizcaíno et al. 2010). If such permanent El Niño-like condition took place, a weak interannual variability of the ISM is expected in the Late Miocene. However, recent geological evidence reveals a persistent interannual ENSO variability in the Pliocene and the preceding periods (Galeotti et al. 2010; Ivany et al. 2011; Scroxton et al. 2011; Watanabe et al. 2011). If such modern-like ENSO variability existed in the Late Miocene, it would then be anticipated that the interannual variability of the ISM might have also been analogous to its present-day state.

In addition to tropical teleconnections (e.g. ENSO), the extratropical forcings also play important roles in driving the interannual variability of the present-day ISM (Yang and Lau 2006). Two types of extratropical forcings have been widely recognized in the modern Asian monsoon system. The first forcing mechanism is the summer wave train responses originating from North Atlantic and Europe, such as the circum-global teleconnection (CGT) (Ding and Wang 2005) and the summer North Atlantic Oscillation (NAO) teleconnection (Syed et al. 2012). The positive (negative) mode of CGT and summer NAO can both induce positive (negative) upper-level geopotential anomalies over west-central Asia, therefore facilitating (suppressing) the low-level convergence over India

(Saeed et al. 2011). The second forcing mechanism is the winter and spring snow cover/depth over Eurasia, which can influence the onset and strength of the ISM by affecting surface albedo over Eurasia, and hence thermal contrast between land and ocean (Barnett et al. 1988; Fasullo 2004; Vernekar et al. 1995). Although the spatial association of snow cover/depth with ISM is complex and is modulated by ENSO and NAO (Robock et al. 2003), a negative relation between winter/spring snow cover over western Eurasia and the ISM has been widely observed (Turner and Slingo 2011; Ye and Bao 2001). Studies have shown that the Late Miocene was much warmer-than-present in the high-latitude Eurasia (Knorr et al. 2011; Lunt et al. 2008; Micheels et al. 2007; Pound et al. 2012; Schneck et al. 2012). Accordingly, the mean Eurasian snow cover in winter and spring might have been much less extensive. Moreover, the atmospheric circulation over North Atlantic in the Late Miocene may have also been distinct from that at present (Eronen et al. 2009, 2012; Micheels et al. 2011). How these changes in extratropical forcings may have affected the interannual variability of the ISM remains obscure.

The fully coupled atmosphere–ocean general circulation models (CGCM) have been successfully applied to investigating the inter-annual climate variability (particularly ENSO) in several pre-Quaternary periods, such as the Eocene (Huber and Caballero 2003), Miocene (Galeotti et al. 2010; Krapp 2012; von der Heydt and Dijkstra 2011) and the mid-Pliocene (Haywood et al. 2007). However, few studies have been focusing on the interannual variability of the Asian monsoons in the deep past. In this study, we use the CGCM ECHAM5/MPI-OM to explore the interannual variation of the ISM and its relation with ENSO and extratropical forcings in the Late Miocene when the mean state of the ISM underwent significant changes. The regional climate model COSMO–CLM with higher spatial resolution is also employed to further capture the spatial structure of the interannual changes, particularly in precipitation. Since the magnitude of the global warming and atmospheric CO<sub>2</sub> concentration in the Late Miocene and Pliocene are likely to be comparable to that in the future (Haywood et al. 2009; Kutzbach and Behling 2004; Lunt et al. 2008), understanding the Asian monsoon climate in these periods may provide insights to its future changes (Utescher et al. 2011).

In this paper, we first describe the models and data in Sect. 2. Then, the changes in the mean state of the ISM, and the temporal and spatial structures of the interannual variation of the ISM in our Late Miocene runs are described in Sect. 3. The tropical and extratropical teleconnections affecting the ISM variability are also analyzed in this section. Finally, in Sect. 4, the possible mechanisms for the interannual variability of the ISM in the Late Miocene are discussed.

## 2 Models and data

### 2.1 Global climate model

Long term simulations for the present-day and the Late Miocene (11–7 Ma, i.e. Tortonian) with the CGCM ECHAM5/MPI-OM (Micheels et al. 2011) are used in this study. They are referred to as GCTRL and GTORT, respectively. Both GCTRL and GTORT runs are integrated over 2,600 years so that the model runs are in their dynamic equilibrium in terms of global mean temperature and sea ice volume. Here we use the last 110-year model integrations for analysis.

ECHAM5/MPI-OM has been regarded as one of the state-of-the-art CGCMs that represent the Asian summer monsoon mean and interannual variability relatively well compared to other CGCMs (Kripalani et al. 2007a, b). The ability of ECHAM5/MPI-OM in representing the Asian summer monsoon variability has been partly attributed to its good performance in simulating the ENSO-related sea surface temperature (SST) variability (Kripalani et al. 2007a). In this study, the resolution of the atmospheric model (i.e. ECHAM5) is T31 (about  $3.75^\circ \times 3.75^\circ$ ) with 19 terrain-following vertical layers. The ocean circulation model (i.e. MPIOM) uses an Arakawa C-grid with an approximate resolution of  $3^\circ \times 3^\circ$  and 40 unevenly spaced vertical levels.

To better represent the climate in the Late Miocene, the physical boundary conditions, such as orography, land–sea distribution and vegetation, were modified in GTORT. Table 1 summarizes the major changes in physical boundary conditions in GTORT. More details can be found in our previous studies by Eronen et al. (2009) and Micheels et al. (2011). Briefly, the orography in GTORT is generally lower than at present. For instance, Greenland is much lower than today because of the removal of the modern ice sheet. The palaeo-elevation of the TP in the Late Miocene is still largely uncertain (Molnar et al. 2010; Yin 2010). Large regional differences in surface uplift of the TP have been reported (Rowley et al. 2001; Spicer et al. 2003; Wang et al. 2008; Zheng et al. 2000). This, however, can not be represented by our global model owing to its coarse resolution. As a result, the TP is generally reduced to 70 % of present-day height. The land–sea distribution in GTORT is largely the same as today. But Australia is two grid cells southward compared to GCTRL (based on Herold et al. 2008). This leads to an open Indonesian Seaway. There is also an open Panama Isthmus with a depth of 500 m in the ocean model of GTORT (based on Collins et al. 1996). In addition, the Paratethys Sea and the Pannonian Lake in Central Eurasia are present in GTORT (based on Harzhauser and Piller 2007; Popov et al. 2006). For vegetation, a proxy-based reconstruction of vegetation (Micheels et al. 2007) is employed. The Tortonian vegetation is characterized by a

larger-than-present forest cover and less desert. Particularly, the present-day deserts in central Asia and Sahara are replaced by grassland and savanna in GTORT. The boreal forests extend far more into the high latitudes including Greenland (see Fig. 2 in Micheels et al. 2011). The  $\text{CO}_2$  concentration in GTORT is set to 360 ppm which is equivalent to present. A wide range of the estimated  $\text{CO}_2$  concentration for the Late Miocene (200–400 ppm) has been reported based on different methods (Beerling and Royer 2011; Bradshaw et al. 2012; Kurschner et al. 2008; Pagani et al. 1999; Pagani et al. 2005; Pearson and Palmer 2000). The value that we chose lies in the range of these estimates, therefore should be reasonable for the Late Miocene. The orbital parameters were also chosen the same as present-day, because the Tortonian covers a time span of 4 million years including many orbital cycles.

### 2.2 Regional climate model

The regional model used in this study is COSMO–CLM, which is the climate mode of a non-hydrostatic regional weather prediction model consortium for small-scale modelling (COSMO) (available at <http://www.clm-community.eu>). It can simulate the mean Asian monsoon circulation and precipitation well compared to other regional climate models (Dobler and Ahrens 2010; Rockel and Geyer 2008) and has been applied in projecting the future mean ISM state (Dobler and Ahrens 2011). Compared to its driving models (e.g. ECHAM5), COSMO–CLM improves not only the spatial patterns of precipitation, but also the temporal correlations of ISM and ENSO (Dobler and Ahrens 2010). This important feature would allow the regional model to capture the interannual variability of the ISM more realistically.

In this study, we use the regional model version 2.4.11 of COSMO–CLM. The configuration of the model parameters are the same as in our previous studies (Tang et al. 2011, 2012). The regional model domain covers the Asian monsoon area ( $0\text{--}60^\circ\text{N}$  and  $50\text{--}140^\circ\text{E}$ ) with a spatial resolution of  $1^\circ \times 1^\circ$  on the rotated model grid and 20 vertical levels. Two regional model simulations are analyzed: a present-day control run (CTRL) and a Tortonian run (TORT). Both experiments are integrated for 110 years. Because the initial adaptation of the upper-level soil moisture in the regional model takes a few months (Tang et al. 2011), the first year integration is left for the model to spin up. We use the last 109-year results for analysis.

The initial and physical boundary conditions for both CTRL and TORT have been described in detail by Tang et al. (2011). For CTRL, we use the last 110-year output of present-day global climate run (i.e. GCTRL) as the initial and lateral boundary forcing. The physical boundary conditions (e.g. land–sea distribution, orography and vegetation) are as at present. In contrast, TORT is driven by the

**Table 1** The setup of the physical boundary conditions for the Tortonian in the global (GTORT) and regional (TORT) climate models (from Tang et al. 2011)

Boundary conditions	GTORT	TORT
Orography	Tibetan Plateau (TP): 70 % (of present-day height) Lower Greenland, Alps and other orography	Northern TP: 30 % (of present-day height) Central and southeastern TP: 80 % Southern TP: 100 % Tian Shan, Gobi Altai and Zagros: 70 % Other orography: 70–90 %
Vegetation	Northward expansion of warm forest Grassland and savanna over central Asia, western Asia and Sahara Boreal forest over the northern high latitudes including Greenland	Northward expansion of temperate deciduous forest in northern Asia Grassland over central Asia Mixed-leaf forest in the southern TP Open forest in the northern TP and the Loess Plateau
Land-sea distribution	Presence of the Paratethys Open Panama Isthmus with a depth of 500 m; southward shift of Australia and open Indonesian seaway	Presence of the Paratethys with the same extent as GTORT
$p\text{CO}_2$	Same as GCTRL (360 ppm)	Same as CTRL (360 ppm)
Orbital parameters	Present-day	Present-day

last 110-year output of the Tortonian global climate run (i.e. GTORT). The physical boundary conditions in TORT are modified to be consistent with that in GTORT (Table 1). However, the orography in TORT is modified in more details owing to the relatively high resolution of the regional model. We keep the southern TP at the present-day height (based on Coleman and Hodges 1995; Rowley et al. 2001; Spicer et al. 2003), but reduce the central TP and the northern TP to 80 and 30 % of their present-day height, respectively (based on Liu-Zeng et al. 2008; Rowley and Currie 2006; Wang et al. 2008; Zheng et al. 2000). For other topography, such as the Tianshan and Zagros Mountains, significant surface uplift during the Late Miocene has been reported (Allen et al. 2004; Charreau et al. 2009; Lacombe et al. 2006). But quantitative palaeoaltimetry studies are very limited. Therefore, their elevations are assumed to be 70 % of their present-day heights. The sensitivity of the ISM to different orographic configurations in our regional model can be found in our previous study (Tang et al. 2012).

### 2.3 Monsoon indices

Various diagnostic indices have been proposed to capture the general intensity of the ISM (Goswami et al. 1999; Parthasarathy et al. 1992; Wang et al. 2001). Although each of them is capable of providing concise yet adequate measures of the ISM individually, the use of only one of these indices may over-simplify the complexity of the ISM system. To comprehensively measure the mean state and the interannual variation of the ISM intensity, four summer

monsoon indices are calculated in this study. (1) All Indian monsoon rainfall index (AIMR) is originally defined by June–July–August–September (JJAS) precipitation (mm) over all of India excluding the four hilly meteorological subdivisions (Parthasarathy et al. 1992). In this study, we use JJA precipitation instead to be consistent with other monsoon indices. (2) The vertical zonal wind shear index (WY) is defined as JJA-mean zonal wind difference (m/s) between 850 and 200 hPa over 60–90°E, 5–20°N (based on Webster et al. 1998). (3) The vertical meridional wind shear index (MH) is defined by JJA-mean meridional wind difference (m/s) between 850 and 200 hPa over 70–110°E, 10–30°N (based on Goswami et al. 1999). (4) The low-level zonal wind shear index (IMI) is JJA-mean zonal wind difference (m/s) between southern (60–80°E, 5–15°N) and northern (70–90°E and 20–30°N) India at 850 hPa (based on Wang et al. 2001). The latter three indices capture different dynamical aspects of the ISM, such as the traverse monsoon circulation (WY), monsoon Hadley circulation (MH) and lower tropospheric vorticity associated with the Indian monsoon trough (IMI), respectively. The averaging areas for WY and IMI are smaller than the original definitions so that they can be applied also to our regional model results.

## 3 Results

### 3.1 Mean ISM state in the Late Miocene

Using a set of adapted Late Miocene boundary conditions, GTORT displays a global annual mean temperature of

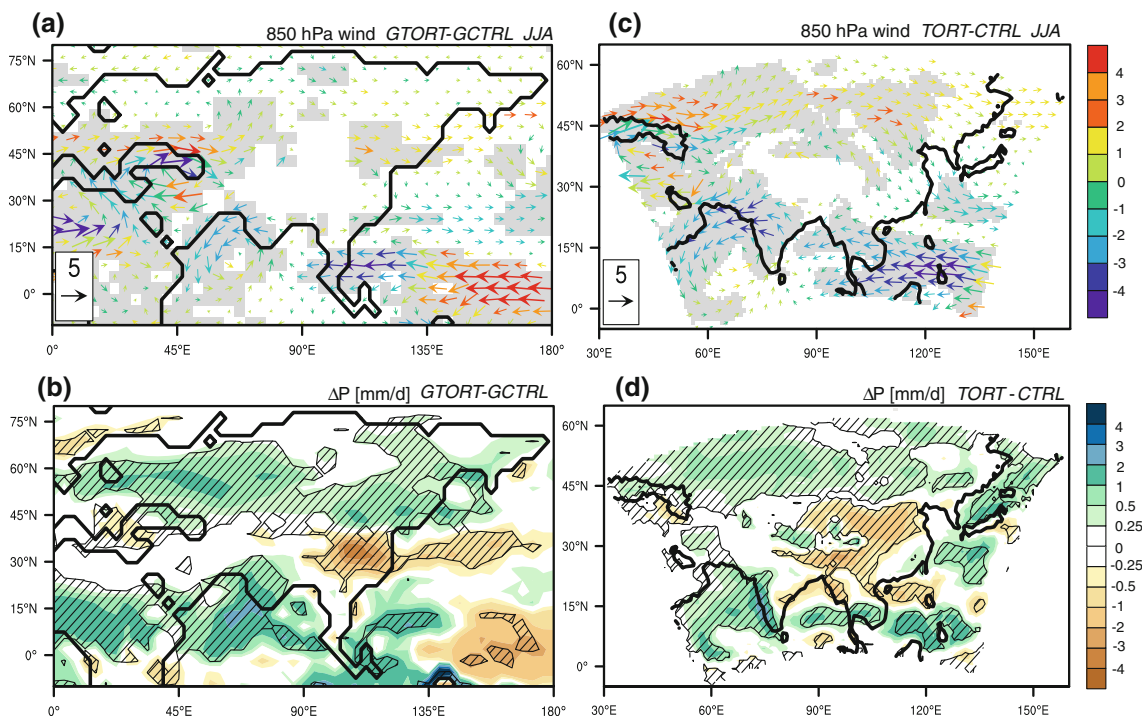


**Fig. 1** The mean summer (JJA) wind anomalies ( $\text{m s}^{-1}$ ) at 850 hPa (**a, c**) and mean annual precipitation anomalies ( $\text{mm day}^{-1}$ ) (**b, d**) between the Tortonian and the present-day control runs (modified from Tang et al. 2011). **a, b** GTORT minus GCTRL.

**c, d** TORT minus CTRL. The *hatched areas* in **b, d** and the *shaded areas* in **a, c** show the significant anomalies with a Student's *t* test ( $p < 0.05$ ). The *colour of vectors* in **a, c** denotes the changes in wind speed

18 °C and annual mean precipitation of 1,110 mm. This is +1.5 °C warmer and +43 mm/year wetter than in GCTRL (Micheels et al. 2011). The performance of the GTORT simulation in relation to proxy data and other models has been analyzed by Micheels et al. (2011) in detail. In respect to mean annual temperature, GTORT agrees well with proxy data in the mid-latitudes, but tends to be slightly too warm in the tropics and too cold in the high-latitudes. This indicates a steeper meridional temperature gradient in GTORT than that suggested by proxy data. Nevertheless, compared to previous Tortonian experiments using ECHAM4 coupled to a mixed-layer ocean model (Micheels et al. 2007; Steppuhn et al. 2007), GTORT produces more pronounced global warming over the high-latitudes, therefore the consistency of GTORT and proxy data has been improved. With respect to annual mean precipitation, GTORT demonstrates good agreement with proxies over central Europe and East Asia. It, however, represents slightly more arid conditions over central Eurasia and the eastern Mediterranean. In general, the results of GTORT show state-of-the-art performance in capturing the Late Miocene climate compared to other Miocene experiments (Bradshaw et al. 2012; Herold et al. 2011; Knorr et al. 2011; Pound et al. 2011; Tong et al. 2009), therefore are warranted for further analysis.

Over the Asian monsoon region, GTORT shows a low-level northerly wind anomaly over East Asia, and an easterly wind anomaly over the South China Sea, the Indian Subcontinent and the Arabian Sea in summer compared to GCTRL (Fig. 1a). This suggests a weakened summer monsoon circulation in both India and East Asia (Tang et al. 2011). Consistent with the weakened summer monsoon circulation, there is a decrease of mean annual precipitation over East Asia in GTORT (Fig. 1b), but precipitation over India increases. This is due to the higher SST over Indian Ocean in GTORT, which leads to a stronger evaporation and a greater moisture advection onto the Indian subcontinent (Micheels et al. 2011). The contradictory changes in ISM precipitation and circulation can also be seen in the alternative monsoon indices (Table 2). While WY suggests weaker monsoon intensity in GTORT, the rainfall index (AIMR) together with MH and IMI indicates a stronger one.

The mean climate anomalies estimated by regional climate model experiments (i.e. TORT-CTRL) are generally in concert with that of the global model (Tang et al. 2011). As illustrated in Fig. 1c, TORT also exhibits a weakened summer monsoon circulation. However, the precipitation anomaly between TORT and CTRL displays more regional differences compared to the global model results. For instance, precipitation decreases in northern China but

**Table 2** The mean and standard deviation of the ISM indices in the global and regional climate model experiments

	AIMR	WY	MH	IMI
<b>GCTRL</b>				
Mean	661	27.00	0.75	8.70
SD	133	1.97	0.82	1.81
<b>GTORT</b>				
Mean	788	25.80	0.96	9.70
SD	128	2.38	0.80	1.97
<i>p</i> value				
Mean <sup>a</sup>	<0.0001	<0.0001	0.05	<0.0001
SD <sup>b</sup>	0.69	0.05	0.78	0.39
<b>CTRL</b>				
Mean	358	25.78	-0.23	7.28
SD	98	2.34	1.07	2.17
<b>TORT</b>				
Mean	364	24.56	-0.11	10.03
SD	113	2.80	1.09	2.37
<i>p</i> value				
Mean	0.69	<0.001	0.41	<0.0001
SD	0.14	0.06	0.86	0.35

Detailed information on the monsoon indices are described in Sect. 2.3 in the text

<sup>a</sup> The significance of difference in mean value between GCTRL (CTRL) and GTORT (TORT) with a Student's *t* test

<sup>b</sup> The significance of difference in standard deviation between GCTRL (CTRL) and GTORT (TORT) with an *F* test

increases in southern China. The increase of precipitation over India mainly occurs in the western coast of India, while its northern part becomes drier in TORT (cf. Fig. 1b, d).

The consistency of the mean summer monsoon state in GTORT and TORT with the Asian monsoon proxies has been discussed in Tang et al. (2011). Both GTORT and TORT are in general concert with the monsoon proxies. For example, the reduced rainfall over northern China in GTORT and TORT (Fig. 1b, d) is consistent with the mammal fossil records which indicate drier-than-present conditions in the Tortonian (Eronen et al. 2010; Liu et al. 2009). The weakened summer monsoon wind over the Arabian Sea (Fig. 1a, c) is also inferred from foraminiferal records in this region (Huang et al. 2007; Kroon et al. 1991). The stronger ISM precipitation in GTORT is more concordant with fossil and chemical records from this region (Clift et al. 2008; Dettman et al. 2001; Hoorn et al. 2000). In contrast, TORT shows better agreement with monsoon precipitation proxies in southern China (Clift et al. 2008) and northwestern India and Pakistan (Quade et al. 1989; Sanyal et al. 2010). This demonstrates the advantage of high-resolution regional climate model in

depicting the spatial difference of monsoon rainfall in the Late Miocene (see more discussion in Tang et al. 2011).

### 3.2 Interannual variability of the ISM in the Late Miocene

#### 3.2.1 Temporal structure

The intensity of the ISM interannual variability can be evaluated by the standard deviations of different monsoon indices (Table 2). The changes of the intensity of the ISM interannual variability in GTORT depend on the monsoonal indices chosen and do not necessarily coincide with the changes of the mean ISM strength. Compared to GCTRL, the standard deviations of AIMR and MH are slightly smaller in GTORT. However, WY and IMI show larger standard deviations (Table 2). Particularly, the increase of standard deviation of WY is significant at 0.05 level. This indicates a similar-to or even stronger-than-present interannual variation of the ISM in the Late Miocene. This trend is further confirmed by the regional model results, which exhibit larger standard deviations of all the monsoon indices in TORT than in CTRL (Table 2).

On interannual scale, all the summer monsoon indices are closely related to each other (Table 3). Particularly, IMI is highly correlated with monsoon rainfall (AIMR) (Fig. 2; Table 3). For simplicity, we choose IMI for the following spectra and composite analyses. Additionally, the spectra of AIMR are shown and discussed in Online Resource. We do not use direct rainfall index (e.g. AIMR) here, because it is usually not well-simulated compared to circulation indices in CGCMs (Fu and Lu 2010).

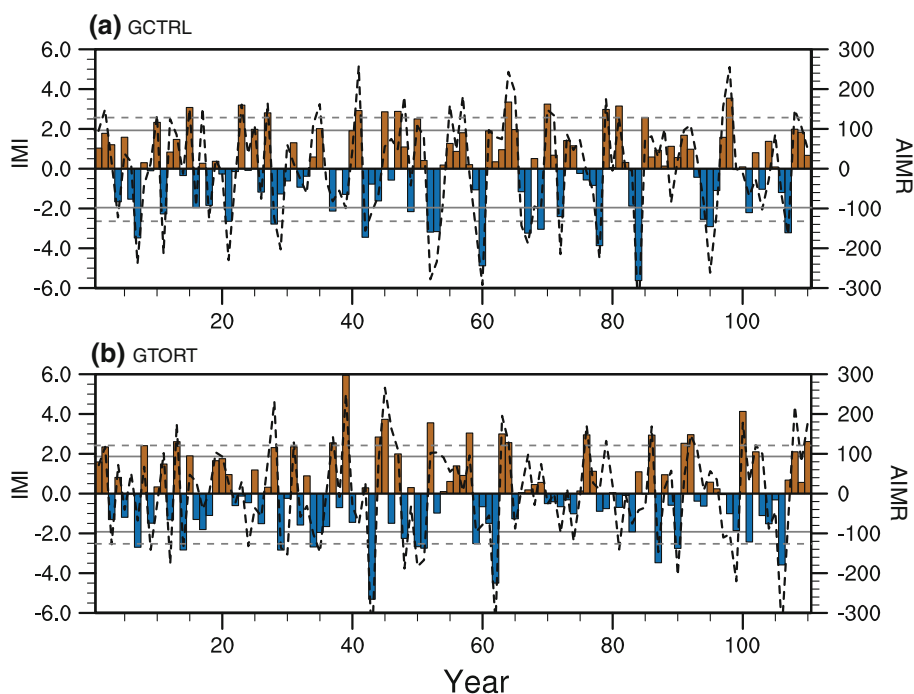
The spectrum of IMI in modern NCEP/NCAR reanalysis data reveals a major variation of the ISM intensity at periods of about 5.5 and 11.1 year (Fig. 3a). The spectrum of IMI in GCTRL has dominant periods in the range of 8–5

**Table 3** Correlation of different monsoon indices in the control (GCTRL and CTRL) and the Tortonian (GTORT and TORT) runs

	AIMR– WY	AIMR– MH	AIMR– IMI	WY– MH	WY– IMI	MH– IMI
GCTRL	0.47	0.89	0.87	0.31	0.57	0.74
GTORT	0.58	0.85	0.81	0.57	0.63	0.65
CTRL	0.53	0.69	0.72	0.52	0.73	0.60
TORT	0.71	0.70	0.81	0.63	0.77	0.66
NCEP	0.44	0.51	0.63	0.31	0.52	<i>0.17</i>

The correlation coefficients of the same monsoon indices based on the homogeneous all-Indian monsoon rainfall data (Parthasarathy et al. 1994) provided by Indian Institute of Tropical Meteorology (<http://www.tropmet.res.in>) and the NCEP/NCAR reanalysis 1 for the period 1948–2010 are also shown as reference. All the correlation coefficients are significant at 0.05 level except those in italics

**Fig. 2** Time series of dynamical index (IMI) (bar) and rainfall index (mm) (AIMR) (line) of the ISM. **a** GCTRL, **b** GTORT. The 11-year Gaussian filter has been applied to remove the variation on decadal scale. The grey horizontal lines denote one standard deviation of IMI (solid) and AIMR (dashed)



years, which is close to that in reanalysis data (Fig. 3b). In contrast, GTORT shows a pronounced variation of IMI at periods of 2.7–2.6 year, indicating a strong quasi-biennial variation of the ISM in the Late Miocene (Fig. 3c). The variation of IMI at a period of  $\sim 9$  year is still significant in GTORT, but is much less dominant compared to that in GCTRL. The spectra of IMI from the regional model results (i.e. CTRL and TORT) are analogous to that in the global model (Fig. 3d, e), even though the dominant periods in CTRL (TORT) are slightly different from that in GCTRL (GTORT).

### 3.2.2 Spatial pattern

To demonstrate the spatial pattern of climate changes associated with the interannual variation of the ISM, the composite differences of summer rainfall (mm/day) and 850 hPa wind (m/s) between the strong and weak ISM years are illustrated in Fig. 4. The strong (weak) ISM years are defined as the years when their IMI is above (below) the average with one standard deviation. In GCTRL, during the strong ISM years, precipitation increases significantly over India and the Bay of Bengal due to enhanced low-level vorticity around this region. Associated with this is a strengthened cross-equatorial southerly flow along the coast of East Africa. There is also an increase of precipitation and southerly wind over northern China, indicating an in-phase change of the East Asian summer monsoon with the ISM (Fig. 4a). Out of the Asian monsoon region, precipitation greatly increases over the eastern tropical Indian Ocean, while it decreases over the western tropical Pacific

accompanied by an easterly wind anomaly there. All the above mentioned patterns are in general agreement with those shown in modern reanalysis data (Fig. 4c; Wang et al. 2001). However, the magnitude of changes in reanalysis data is much smaller (cf. Fig. 4a, c) and less significant. Particularly, the southerly wind anomaly over East Asia and the easterly wind anomaly over western tropical Pacific are hardly visible in reanalysis data (Fig. 4c). The composite differences in GTORT are quite similar to that in GCTRL (Fig. 4b). A small difference is that the increase of precipitation over East China is more extensive in GTORT than in GCTRL during the strong ISM years.

The composite differences between strong and weak ISM years in the regional model broadly agree with those of the global model (Fig. 5). Nevertheless, some meso-scale structures of precipitation changes, which are not visible in the global model, are more clearly manifested in the regional model. For instance, a zonal elongated band of strong summer rainfall increment over northern China during strong ISM years is seen in both CTRL and TORT (Fig. 5). Such a band of strong rainfall increment moves southward in TORT compared to CTRL (cf. Fig. 5a, b). This can be due to the southward displacement of the mean position of the subtropical rain front (referred to as Meiyu front in June and July in China) in TORT owing to the lower TP (Tang et al. 2011). It is also noticed that precipitation variations over northwestern India are smaller in TORT than in CTRL, which may be related to the weaker mean summer monsoon rainfall in this region in TORT. In general, it seems that the high-resolution regional model experiments do not provide much additional information on the spatial structure of the

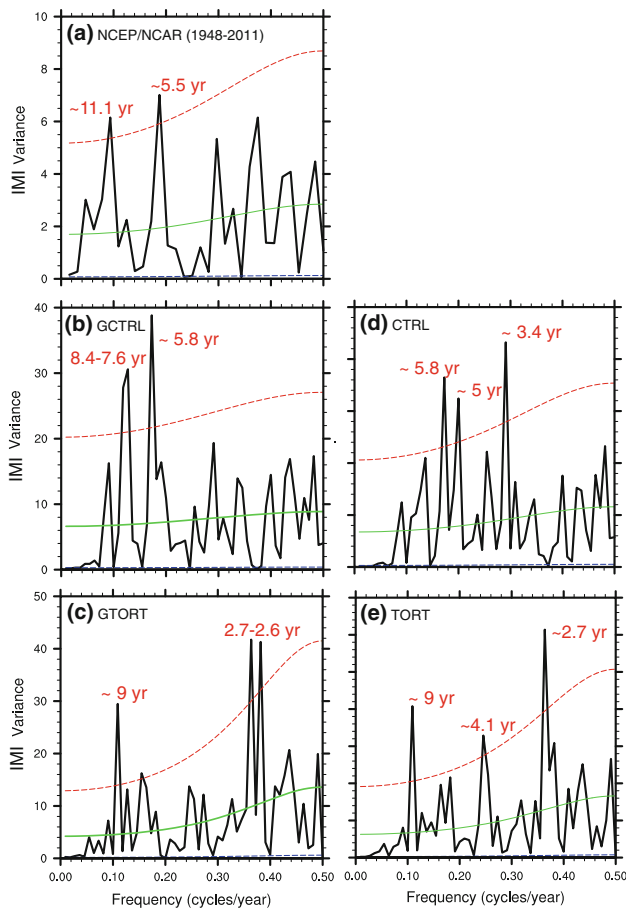


**Fig. 3** Spectra of dynamical ISM index (IMI) in **a** NCEP/NCAR reanalysis 1 for the time period 1948–2011 (Kalnay et al. 1996). The data are obtained from the NOAA/OAR/ESRL PSD, Boulder, CO, USA (<http://www.esrl.noaa.gov/psd/>). **b** GCTRL, **c** GTORT, **d** CTRL, **e** TORT. The smooth coloured curves are the red noise spectrum and its 95 % confidence level. The 11-year Gaussian filter has been applied to remove the variation on decadal scale before spectral analysis

interannual variation of the ISM. This is in contrast to the fact that the regional model produces greater regional difference in the mean monsoon rainfall changes than the global model (cf. Fig. 1b, d), therefore implying that the interannual variation of the Asian monsoon rainfall might be largely modulated by external global forcings and large-scale circulation rather than the local dynamical processes within the monsoon region.

To demonstrate the major spatial pattern of the interannual variation, we also performed an empirical orthogonal function (EOF) analysis on summer precipitation and 850 hPa wind over the Asian monsoon region (0–60°N, 60–150°E). The first EOF modes, which account for more than 40 % of the total variance in both GCTRL and GTORT (Fig. S2 in Online Resource), are quite similar to that depicted by the composite differences between strong and weak ISM years (Figs. 4, 5). This, hence, confirms the

spatial pattern of the interannual variation of the ISM described in Figs. 4 and 5.

### 3.2.3 ENSO and ENSO–ISM relation

The interannual variation of ENSO is a salient feature of the present-day climate system. The observed spectrum of the monthly El Niño index (i.e. NINO 3.4; 1854–2010) shows a prominent irregular variation at periods of 3–7 years (Fig. 6a). The spectrum of NINO 3.4 in GCTRL (Fig. 6b) is close to the observed spectrum, but exhibits a major variation at shorter periods (about 3.5–2 years). This has been found to be a common bias in many CGCMs (e.g. von der Heydt and Dijkstra 2011). Compared to GCTRL, the spectrum of NINO 3.4 in GTORT displays a major period focusing at 2.8–2.5 year (Fig. 6c). This suggests a more periodic ENSO variability in the Late Miocene. The standard deviations of three different El Niño indices (NINO3, NINO3.4 and NINO4) all show higher values in GTORT in all four seasons except spring (Table 4). This points to a larger amplitude of ENSO in the Late Miocene than at present (particularly in the summer season). The El Niño events have been divided into central Pacific (i.e. El Niño Modoki) and eastern Pacific types (Yeh et al. 2009). The ratio of the occurrence of central and eastern Pacific El Niño events is 2.27 in GCTRL and 2.43 in GTORT. This suggests no apparent shift in the spatial pattern of ENSO variability between GCTRL and GTORT.

The connection between ENSO and the interannual variation of the ISM can be displayed by the composite difference of surface temperature between strong and weak ISM years (Fig. 7). In GCTRL, strong ISM is associated with the decline of summer SST over the central and eastern tropical Pacific, and the increase of summer SST over the western tropical Pacific, such as the Philippine Sea. This suggests La Niña conditions during the strong ISM years, which is consistent with modern observations (Fig. 7c; Gadgil 2003). However, the decrease of SST over the central and eastern tropical Pacific in GCTRL is too strong and extends too far into the western Pacific during the strong ISM years (cf. Fig. 7a, c). This is known as the cold tongue bias, which has been noticed in many CGCMs including ECHAM5/MPIOM (Guilyardi 2006; Guilyardi et al. 2009; Jungclaus et al. 2006; Lu et al. 2008; Muller and Roeckner 2008). In GTORT, the surface temperature anomalies during the strong ISM years resemble that in GCTRL (Fig. 7b). The decrease of SST over the central and eastern tropical Pacific is even stronger and more meridionally confined in GTORT. This indicates a persistent or even stronger ENSO–ISM relation in GTORT.

Figure 8 further illustrates the lead-lag correlation between NINO3.4 and IMI. It shows that IMI is most negatively related to NINO3.4 in the same summer season. Such



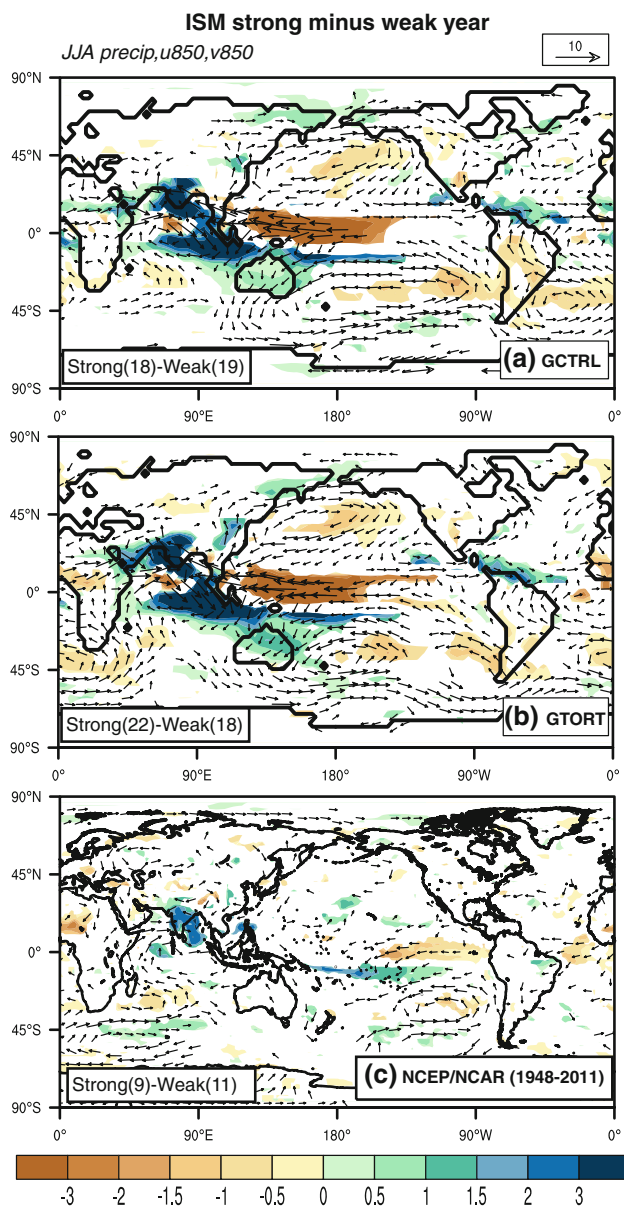


**Fig. 4** Composite difference of summer rainfall (mm/day) and 850 hPa wind (m/s) between the strong and weak ISM years with respect to IMI. **a** GCTRL, **b** GTORT, **c** NCEP/NCAR reanalysis 1 for the time period 1948–2011. The precipitation differences significant with a Student’s *t* test ( $p < 0.05$  in **a** and **b**,  $p < 0.1$  in **c**) are colour shaded. The wind anomalies that either the zonal or meridional wind difference is significant with a Student’s *t* test ( $p < 0.05$  in **a** and **b**,  $p < 0.1$  in **c**) are denoted by black vector. The number of years selected for computing the strong/weak composites are annotated in the bottom-left corner of each figure

negative relationship seems to remain in the preceding and following winter season in both GCTRL and GTORT. This is in contrast to the reanalysis data which indicates a sudden shift to a positive correlation between IMI and NINO3.4 in the preceding winter season (Fig. 8). Such bias can be better detected in Fig. 9 which illustrate the annual evolution of

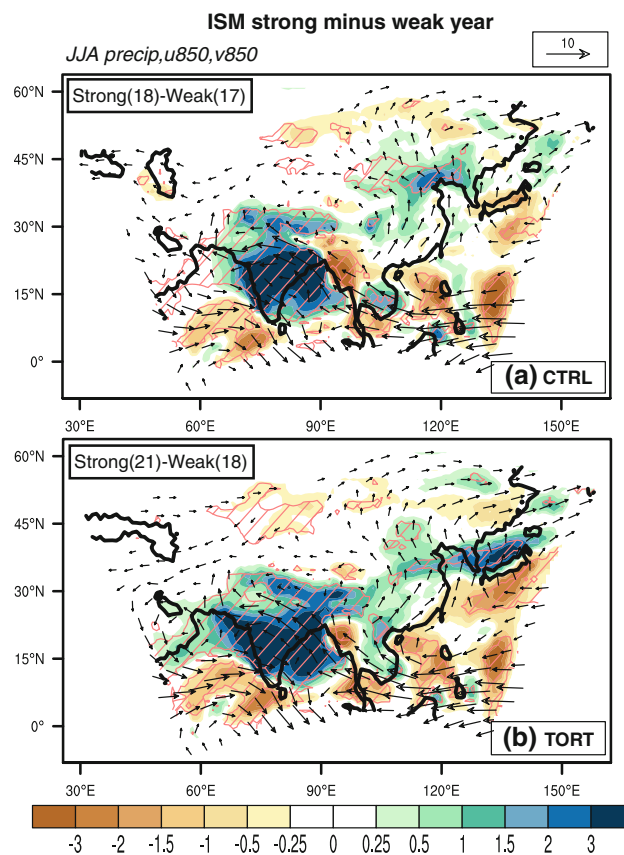


**Fig. 5** As in Fig. 4, but for the regional climate model results. **a** CTRL, **b** TORT. The precipitation differences significant with a Student’s *t* test ( $p < 0.05$ ) are hatched

NINO3.4 anomalies associated with different ISM and ENSO strength. In reanalysis data, the strong negative (positive) ENSO events in summer all begin with a positive (negative) ENSO in the preceding winter (Fig. 9c). This accounts for the reversed sign of the correlation coefficients between IMI and NINO3.4 from preceding winter to summer (Fig. 8). Our global model well captures the shift of ENSO phase from positive in winter to strong negative in summer (black and blue lines in Fig. 9a, b). However, a positive ENSO almost persists throughout the year when the ISM is prominently weak (green and purple line in Fig. 9a, b). This mainly contributes to the persistent negative correlation between IMI and NINO3.4 in the preceding winter in both GCTRL and GTORT (Fig. 8). Compared to GCTRL, GTORT shows more prominent transition of ENSO status from winter to summer. Even in the normal monsoon and ENSO years, a reverse of ENSO phase in spring is visible (dashed lines in Fig. 9b). This suggests a stronger biennial oscillation of ENSO in GTORT. As a result, IMI in GTORT shows stronger positive correlations with NINO 3.4 in the winter season 1 year before and in the summer and winter 1 year after (Fig. 8).

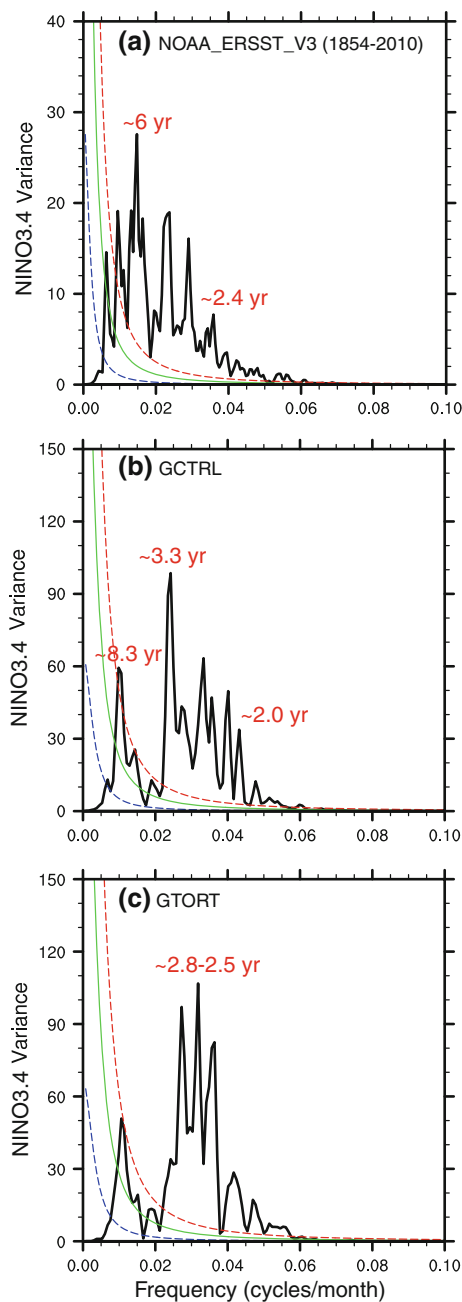


**Fig. 6** Spectra of monthly El Niño index (NINO 3.4) in **a** NOAA extended reconstructed sea surface temperature (NOAA\_ERSST\_V3b) (Smith et al. 2008) for the time period 1854–2010. The data are obtained from the NOAA/OAR/ESRL PSD, Boulder, CO, USA, through their Web site (<http://www.esrl.noaa.gov/psd/>). **b** GCTRL, **c** GTORT. NINO 3.4 is defined as the sea surface temperature averaged over 170–120°W and 5°S–5°N. The annual cycle has been removed and the 11-year Gaussian filter has been applied to remove the variation on decadal scale. The smooth coloured curves are the red noise spectrum and its 95 % confidence level

### 3.2.4 Extratropical forcings and the ISM

The summer NAO is an important extratropical forcing for the interannual variation of the ISM (Syed et al. 2012).

**Table 4** The standard deviation of seasonal mean El Niño indices in GCTRL and GTORT

	DJF	MAM	JJA	SON
GCTRL				
NINO3	1.34	0.88	1.31	1.13
NINO3.4	1.58	1.11	1.29	1.61
NINO4	1.81	1.26	1	1.97
GTORT				
NINO3	1.43	0.75	1.74	1.35
NINO3.4	1.64	0.89	1.78	1.73
NINO4	1.82	1.13	1.36	2.16
<i>p</i> value <sup>a</sup>				
NINO3	0.50	0.10	0.003	0.07
NINO3.4	0.70	0.02	0.001	0.45
NINO4	0.95	0.26	0.002	0.34

NINO4: SST over 160°E–150°W, 5°S–5°N; NINO3.4: SST over 170°W–120°W, 5°S–5°N; NINO3: SST over 150°W–90°W, 5°S–5°N

<sup>a</sup> The significance of difference in standard deviation between GCTRL and GTORT with an *F* test

To depict NAO and its relation to ISM strength, a NAO index defined by the difference of zonal-averaged (80°W–30°E) sea level pressure between 35°N and 65°N (Li and Wang 2003) is used. The mean value of NAO index in all four seasons is larger in GTORT than in GCTRL (Table 5), suggesting a mean positive NAO-like condition in the Late Miocene (Eronen et al. 2009, 2012; Micheels et al. 2011). However, the standard deviation of NAO is smaller in GTORT than in GCTRL in all four seasons (Table 5), indicating a weakened NAO on interannual scale in the Late Miocene. Interestingly, such stabilization of NAO under a positive NAO-like mean state has also been found in the experiments with increasing greenhouse-gas concentration for future (Paeth et al. 1999). This implies that similar processes may occur in both the Late Miocene and the future that lead to the weakened extratropical climate variability and a stabilized zonal state over North Atlantic.

The correlation coefficients between summer NAO index and the ISM indices are shown in Table 6. Before correlation analysis, the covariance of these indices with summer NINO3.4 has been removed so as to obtain the independent influence of NAO on the ISM strength. It displays that the summer NAO index is positively correlated with all the ISM indices in GCTRL. Particularly, the correlation with IMI is highest and significant at the 0.05 level. This is in concert with that of the reanalysis data (Table 6), demonstrating a significant influence of summer NAO (independent of ENSO) on the interannual variation of the ISM at present day. In contrast, the correlations become much weaker and even negative in GTORT (Table 6).

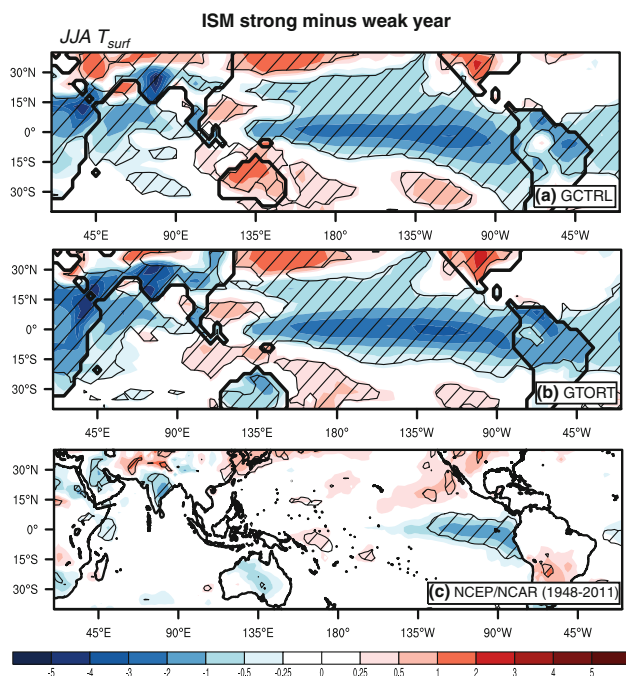


**Fig. 7** Composite difference of summer surface temperature ( $^{\circ}\text{C}$ ) between the strong and weak ISM years. **a** GCTRL, **b** GTORT, **c** NCEP/NCAR reanalysis 1 for the time period 1948–2011. The hatched area denotes the significant difference with a Student's  $t$  test ( $p < 0.05$ ). The strong (weak) ISM years are defined as in Fig. 4

This suggests that the modern summer NAO-ISM connection may have not established in the Late Miocene. Further analysis reveals that this can be ascribed to the absence of North Atlantic forcing in the Late Miocene to sustain a modern-like circumglobal teleconnection (CGT) (Ding and Wang 2005) that modulates the ISM (see Fig. S3 in Online Resource).

To assess the influence of the preceding winter and spring conditions over Eurasia on the ISM, the composite differences of winter and spring surface temperature between strong and weak ISM years are illustrated in Fig. 10. As a good proxy for snow cover, it has been found that the higher (lower) than normal winter and spring temperature can result in a strong (weak) ISM by modifying meridional thermal contrast between land and ocean (Chang et al. 2001; Peings and Douville 2010). Consistent with previous studies, strong ISM years in GCTRL are associated with a positive temperature anomaly over most of Eurasia in the preceding winter. The increase of temperature is most pronounced in East Asia (Fig. 10a), indicating a weakened East Asian winter monsoon before a strong ISM. In spring, there is also a positive temperature anomaly over northern Eurasia, particularly Europe (Fig. 10b).

Compared to GCTRL, the strong ISM years in GTORT are associated with much less extensive positive

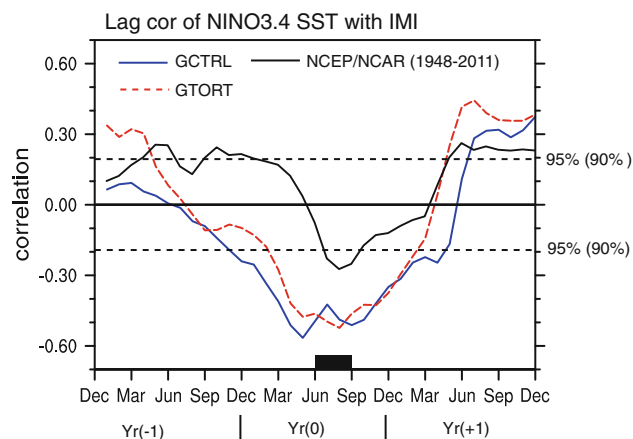


**Fig. 8** Lead-lag correlation coefficients between monthly-mean NINO3.4 index and JJA-mean IMI in GCTRL (blue), GTORT (red) and NCEP/NCAR reanalysis 1 (black). The grey dashed lines denote the 95 % (approximately 90 %) confidence level for GCTRL and GTORT (NCEP/NCAR reanalysis 1)

temperature anomaly over Eurasia in both winter and spring (Fig. 10c, d). This implies a weaker correlation between winter/spring Eurasian conditions and the ISM strength. This can be attributed to the weak winter and spring NAO on interannual scale in GTORT (Table 5). It may also be related to the less snow cover and the weakened snow cover-temperature feedback in GTORT owing to the lower TP and the warmer high latitudes. As a consequence, the influence of extratropical conditions in preceding winter and spring on the ISM seems to be much reduced in GTORT.

#### 4 Discussion

Our modeling results suggest a persistent or even stronger interannual variability of the ISM in GTORT. While the spatial pattern of the interannual variation in GTORT resembles that in GCTRL, the dominant periods of the ISM variation is shorter in GTORT than in GCTRL. We attribute these changes mainly to the stronger and more regular ENSO in GTORT (Table 4; Fig. 6). In addition, the impact of extratropical forcings, such as summer NAO and Eurasian temperature in preceding winter and spring, on the ISM is weak in GTORT (Table 6; Fig. 10). This leads to a stronger ENSO-ISM relationship, therefore the stronger interannual variation of the ISM in GTORT with a prominent 2.7–2.6 year cycle (Fig. 3c) which is identical to the major cycle of NINO 3.4 (Fig. 6c). Compared to GTORT, the ENSO variability in GCTRL is weaker and more irregular (Fig. 6b), while the extratropical forcings exert stronger independent influence on the ISM. Accordingly, the control of ENSO on the interannual variation of the

**Fig. 9** Annual evolution of NINO3.4 in different types of ISM and ENSO years. **a** GCTRL, **b** GTORT, **c** NCEP/NCAR reanalysis 1 for the time period 1948–2011. *norISM*: normal ISM year (JJA-mean IMI is within 1 SD of its average, “±” denotes that IMI is above/below the average). *strISM* (*wkISM*): strong (weak) ISM year (JJA-mean IMI is above (below) the average with at least 1 SD). *norENSO*: normal ENSO year (JJA-mean NINO3.4 is within 1 SD of its average, “±” denotes NINO3.4 is above/below the average). *strENSO* (*wkENSO*): strong (weak) ENSO year (JJA-mean NINO3.4 is above (below) the average with at least 1 SD)

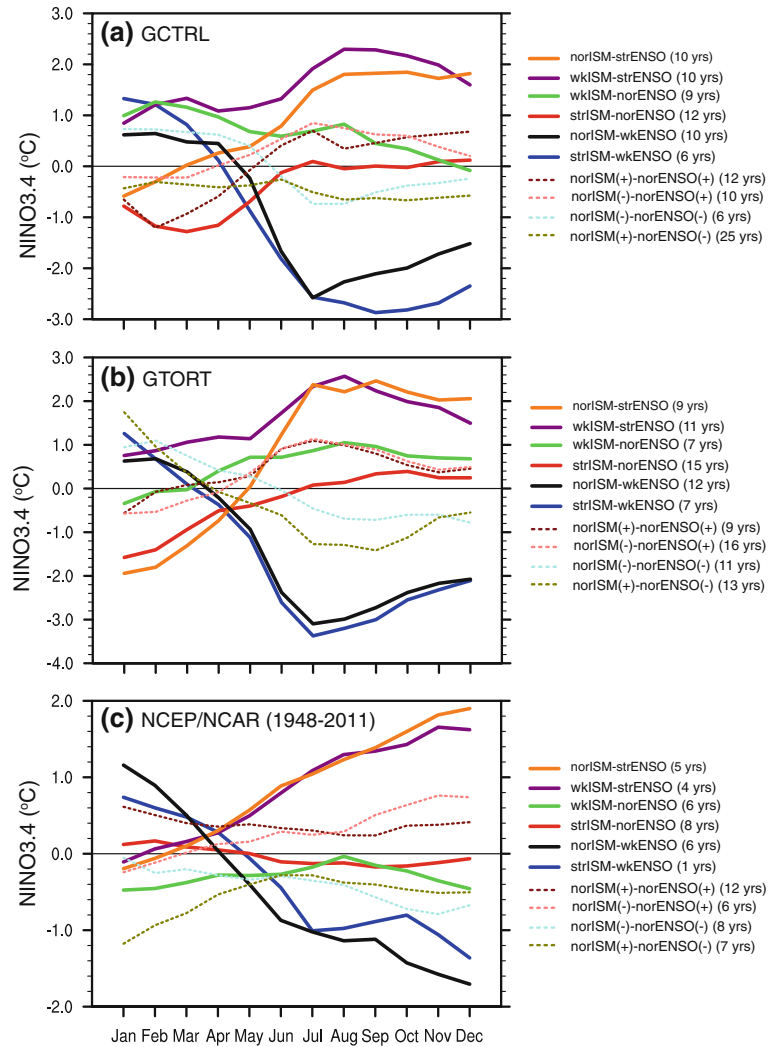


**Table 5** The seasonal mean and standard deviation of North Atlantic Oscillation (NAO) index (Pa) in GCTRL and GTORT

	DJF	MAM	JJA	SON
<b>GCTRL</b>				
Mean	1,446	821	942	1,317
SD	595	396	189	308
<b>GTORT</b>				
Mean	1,681	1,097	1,229	1,775
SD	561	364	163	289
<i>p</i> value				
Mean <sup>a</sup>	0.003	<0.001	<0.001	<0.001
SD <sup>b</sup>	0.54	0.38	0.12	0.51

<sup>a</sup> The significance of difference in mean value between GCTRL and GTORT with a Student’s *t* test

<sup>b</sup> The significance of difference in standard deviation between GCTRL and GTORT with an *F* test

ISM is probably weakened (Fig. 8). This may explain the departure of the major periods of IMI (5–8 year) from that of NINO3.4 (3.3–2 year) in GCTRL.

**Table 6** Correlation of summer (JJA) North Atlantic Oscillation (NAO) index with ISM indices

	NAO–AIMR	NAO–WY	NAO–MH	NAO–IMI
GCTRL	0.15	0.17	0.17	<b>0.22</b>
GTORT	–0.12	0.04	–0.06	–0.16
CTRL	0.11	0.17	0.15	<b>0.23</b>
TORT	–0.13	–0.002	–0.1	–0.12
NCEP	0.15	0.12	–0.03	<b>0.28</b>

The covariance of NAO index and ISM indices with NINO3.4 has been removed before correlation analysis in order to obtain independent influence of NAO on the ISM. The correlation coefficients significant at 0.05 level is denoted in bold. The correlation coefficients based on NCEP/NCAR reanalysis 1 for the period 1948–2010 are also shown as reference

Our model results point to a persistent and even more regular ENSO variability in the Late Miocene. This is in contrast with previous studies that indicate a permanent El Niño-like condition before the Pliocene (Fedorov et al. 2010; Molnar and Cane 2002; Wara et al. 2005). Recently

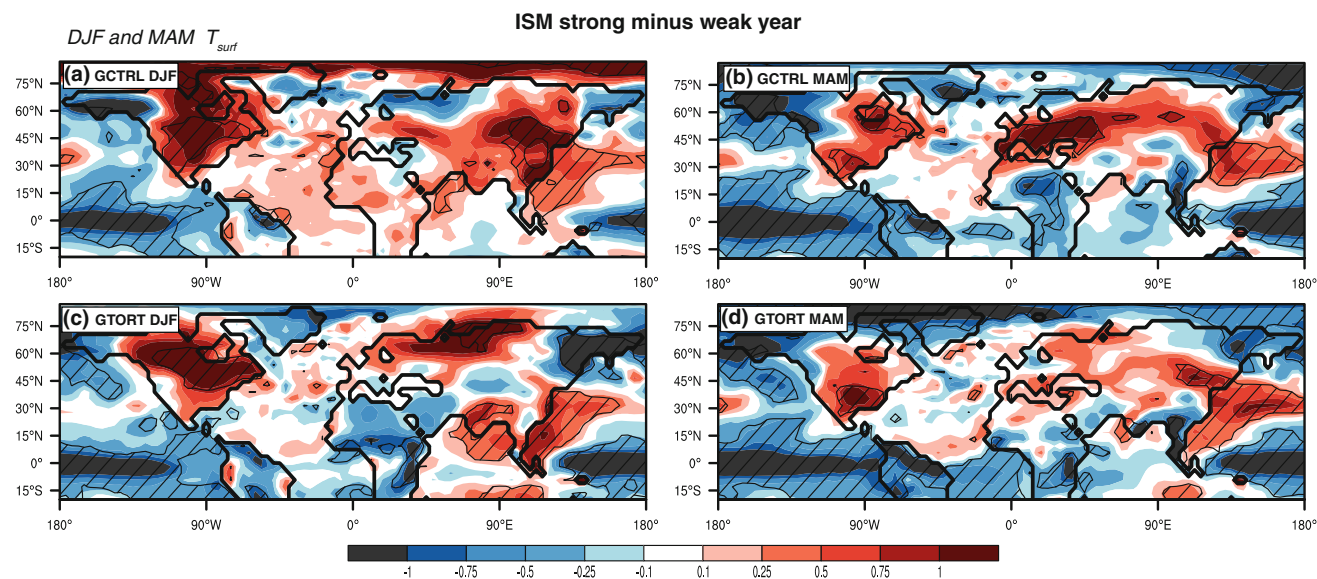


**Fig. 10** Composite difference of winter (DJF) and spring (MAM) surface temperature ( $^{\circ}\text{C}$ ) between the strong and weak ISM years. **a** GCTRL DJF, **b** GCTRL MAM, **c** GTORT DJF, **d** GTORT MAM.

retrieved proxy data, however, reveal that the interannual behavior of ENSO in the Pliocene and the previous periods might have been analogous to the present day (Galeotti et al. 2010; Ivany et al. 2011; Scroxton et al. 2011; Watanabe et al. 2011). These results have been supported by several CGCMs experiments (Table 7). Using CCSM, Huber and Caballero (2003) found a stronger-than-present ENSO variability in their Eocene simulation, and Galeotti et al. (2010) and von der Heydt and Dijkstra (2011) also found a stronger ENSO variability in their Miocene run. Similar results are also observed in the Mid-Pliocene simulation with HadCM3 by Haywood et al. (2007). Our Late Miocene run shows consistent results with these studies, even though we use a different model and different boundary conditions (Table 7). It is interesting to note that Galeotti et al. (2010) reported a stronger teleconnection between ENSO and precipitation in central Europe in their Miocene run. This is also observed in our Late Miocene run (see Fig. S4 in Online Resource).

There are several mechanisms that may contribute to the stronger and more regular ENSO in our Late Miocene run. It can be related to the presence of open Panama and Indonesian Seaways in GTORT (An et al. 2012; Jochum et al. 2009; von der Heydt and Dijkstra 2011). von der Heydt and Dijkstra (2011) have shown that these open ocean gateways can enhance the amplitude of ENSO variability. They attributed this to the stronger atmosphere–ocean coupling in the wider Indo-Pacific ocean basin where ENSO develops. They also found a less frequent ENSO in response to the open ocean gateways (von der Heydt and Dijkstra 2011). This, however, is not observed in our study.

The *hatched area* denotes the significant difference with a Student's *t* test ( $p < 0.05$ ). The *strong* (*weak*) ISM years are defined as in Fig. 4

Such discrepancy can be due to the different CGCM used in our study. Also, it can be related to the different boundary conditions prescribed in our experiments. For instance, we have much smaller opened Indonesian and Panama Seaways in GTORT compared to the Miocene run in von der Heydt and Dijkstra (2011). This may affect the extent of tropical Pacific ocean basin and circulation, possibly limiting the cycle of ENSO. We also have relatively realistic representation of orography for the Late Miocene (Table 1), while an idealized flat topography was used for both the present-day and Miocene runs by von der Heydt and Dijkstra (2011). The changes in orography between our GCTRL and GTORT may also affect ENSO variability (see discussion below), therefore obscure the influence of open seaways as shown by von der Heydt and Dijkstra (2011).

It has been reported that the weakened thermohaline circulation could favor a stronger ENSO variability and ENSO–ISM relationship (Dong and Sutton 2007; Lu et al. 2008). This can be related to the changes in the mean climate state, which is characterized by warmer SSTs/enhanced precipitation in the western Indian Ocean and colder SSTs/reduced precipitation in the eastern Indian Ocean and the western tropical Pacific in summer. The thermohaline circulation is found to be weaker in GTORT than in GCTRL due to the weakened North Atlantic warm current as a result of the open Panama Isthmus (Micheels et al. 2011). This may contribute to the strengthened ENSO and ENSO–ISM relation in GTORT.

Kitoh (2007) has discovered that lower global orography can result in a strong and more periodical ENSO variability.

**Table 7** Summary of the CGCM studies on the interannual climate variability in the warm periods of the deep past and of the future (2100 AD)

	Eocene (Huber and Caballero 2003)	Early- and Mid-Miocene (Galeotti et al. 2010; von der Heydt and Dijkstra 2011) <sup>a</sup>	Late Miocene (this study)	Middle Pliocene (Haywood et al. 2007)	Future (2100 AD)
Model	CCSM 1.4	CCSM 1.4	ECHAM5/MPI-OM	HadCM3	Multi-CGCM
Boundary conditions	CO <sub>2</sub> : 560 ppm	CO <sub>2</sub> : 710 ppm	CO <sub>2</sub> : 360 ppm (this study) CO <sub>2</sub> : 280 ppm (Knorr et al. 2011)	CO <sub>2</sub> : 400 ppm	A1B: CO <sub>2</sub> : 700 ppm in 2100 A2: CO <sub>2</sub> : 850 ppm in 2100
Mean climate	Eocene topography, bathymetry, and vegetation  ~10 °C warmer than today in high latitudes, and much less warmer in the tropics	Idealized Miocene vegetation and soil; open Panama and Indonesian seaways; flat topography  3.5 °C warmer than today (globally)	Late Miocene topography, bathymetry, vegetation and vegetation (see Table 1)  1.5 °C warmer than today (this study) 3 °C warmer than today (Knorr et al. 2011) Weaker ISM circulation but stronger ISM rainfall than today	Pliocene topography and vegetation  ~3 °C warmer than today Weaker ISM rainfall than today	Present-day topography and vegetation  A1B: 2.8 °C warmer than today A2: 3.4 °C warmer than today (IPCC 2007) Weaker ISM circulation but stronger ISM rainfall than today (Kripalani et al. 2007b; Paeth et al. 2008) versus weaker ISM circulation and rainfall than today (Ashfaq et al. 2009; Doblner and Ahrens 2011)
Interannual variability	Stronger ENSO variability than today; similar periodicity to today; similar spatial pattern of ENSO teleconnection to today	Stronger amplitude but less frequent ENSO variability than today; similar spatial pattern of ENSO teleconnection to today	Stronger and more regular ENSO variability than today; similar spatial pattern of ENSO teleconnection to today  Stronger-than-today variability of ISM circulation; similar-to-today variability of ISM rainfall; stronger ENSO-ISM teleconnection than today  Weaker NAO variability than today; weaker summer NAO-ISM teleconnection; weaker winter/spring Eurasian temperature and ISM connection than today	Stronger ENSO variability than today  Stronger ENSO variability than today	Stronger ENSO variability than today (Fu and Lu 2010) versus Large uncertainty on ENSO variability in the future (Collins et al. 2010) Stronger-than-today variability of both the ISM circulation and rainfall (Fu and Lu 2010) Stronger ENSO-ISM relation (Fu and Lu 2010) versus weaker ENSO-ISM relation than today (Kripalani et al. 2007) Weaker NAO variability than today (Paeth et al. 1999)

<sup>a</sup> Galeotti et al. (2010) study the Late Miocene, however, they use the same modeling experiment as in von der Heydt and Dijkstra (2011) which has been regarded as an early Miocene simulation

This is ascribed to the weakened mean easterly trade winds and a widening of the meridional extent of the equatorial wind-ocean response when the mountains are low. In GTORT, the global orography (particularly the TP) is generally reduced (Table 1). This probably promotes ENSO variability, and thus enhances the interannual variability of the ISM in GTORT. Moreover, the lower TP and the surrounding orography in GTORT (TORT) can directly modify the mean state of the ISM, which by itself may exert profound impact on the interannual variability of the ISM (Wu and Ni 1997), particularly its spatial patterns (see discussion in Sect. 3.2.2).

The atmospheric CO<sub>2</sub> concentration and the magnitude of global warming in the Miocene–Pliocene have been considered to be analogous to possible future warming (Haywood et al. 2009; Kutzbach and Behling 2004; Lunt et al. 2008). Under the emission scenarios A1B and A2, the atmospheric CO<sub>2</sub> concentration will arrive at 700 and 850 ppm in year 2100. Multi-CGCM simulations produce a +2.8 and +3.4 °C warming of the global mean surface temperature, respectively and significantly reduced meridional temperature gradient in the future (IPCC 2007). This resembles that observed in our Late Miocene simulation and other Miocene and Pliocene experiments (see Table 7). Although the global warming in the Late Miocene may have been induced by the factors other than CO<sub>2</sub> (e.g. vegetation, topography and land–sea distribution) (Bradshaw et al. 2012), understanding how climate operates in such warm world in general sense would provide useful insights to the future climate changes.

The projection for the ENSO variability under increasing atmospheric CO<sub>2</sub> concentration in the future remains uncertain (Collins et al. 2010; Paeth et al. 2008). However, the majority of the CGCMs including ECHAM5/MPI-OM, have predicted an enhanced ENSO variability (Muller and Roeckner 2008). A strengthened interannual variability of the ISM (Fu and Lu 2010; Kripalani et al. 2007b) and a closer ENSO–ISM relationship (Fu and Lu 2010) in the future have also been predicted by multi-CGCM experiments. Kripalani et al. (2007b) found a weakened ENSO–ISM relation in the future. This is most likely because their analyses are based on only the last 20 years of future simulations, which may be biased because of the decadal variation of the ENSO–ISM relationship.

The future changes in ENSO and ISM variability are surprisingly similar to that found in our Late Miocene runs and other CGCM simulations for similar warm geological periods (Table 7). Such close resemblance may either be a coincidence, or simply suggest that a stronger ENSO and ENSO–ISM relationship might be a robust pattern in a warm climate. Several processes might be responsible for such tendency. For instance, a reduced meridional temperature gradient may maintain a mean circulation

(e.g. weak Walker circulation) favorable for stronger ENSO variability. The warmer high-latitudes may exhibit less climate variability (e.g. weakened NAO variability), therefore less disruption on ENSO and ENSO–ISM relation. Owing to the strong ENSO variability, the interannual variability of ISM may have been stronger than at present in the deep past, even though the lower TP and the surrounding orography at that time may have favored a weak mean ISM and also likely a less developed interannual variability of the ISM.

## 5 Conclusions

The long term simulations of the Late Miocene climate by a CGCM and a regional climate model show that although the mean ISM circulation may have been weaker in the Late Miocene primarily due to the lower TP, its interannual variation may have been similar to or even stronger than today. The spatial pattern of precipitation and low-level wind changes on interannual scale may have remained the same in the Late Miocene as at present. The high-resolution regional model experiments do not provide much additional information on the spatial structure of the interannual variation of the ISM. This implies that the interannual variation of the ISM might be largely controlled by external global forcings and large-scale circulation rather than by local dynamical processes within the monsoon region.

The strong ISM variability in our Late Miocene runs can be largely attributed to the stronger and more periodical ENSO variability, which maintains a tighter ENSO–ISM relation. In addition, the extratropical influence on the ISM variability is weaker, which may further facilitate a strong ENSO–ISM relationship. The persistent and strong ENSO variability in our Late Miocene run may result from the combined effect of the open Panama and Indonesian seaway, the weakened thermohaline circulation, the lower global orography and the warmer global climate.

Finally, we note several limitations of our study. Firstly, we use only one CGCM experiment, and thus the results may be subjected to that model's biases. For instance, our model simulates too strong and too much westward SST anomalies over central and eastern Pacific associated with ENSO. Such bias may overemphasize the influence of ENSO on ISM in both the present-day and the Late Miocene runs. Furthermore, large uncertainties still remain about the boundary conditions for the Late Miocene, such as orography and vegetation. More experiments with different boundary conditions for the Late Miocene and using different CGCMs are necessary to fully evaluate the reliability of our results. In spite of these deficiencies, our results exhibit good agreement with available annually

resolved proxies, which manifest a strong ENSO and its teleconnection in the Late Miocene (see Fig. S5 in Online Resource). The consistency between our Late Miocene run and other CGCM simulations for geological warm periods also support the fidelity of our modeling results, and implies that a strong ENSO and ENSO related teleconnection (e.g. ENSO–ISM relation) may be a robust pattern in geological warm periods as well as future warming climate. The dynamical processes recognized in geological warm periods, therefore, are likely to be responsible for the future changes in climate variabilities.

**Acknowledgments** We thank the Ella and Georg Ehrnrooth foundation for project funding. This work was also supported by the Humboldt Foundation (JTE) and the federal state Hessen (Germany) within the LOEWE initiative (AM). This is a contribution to the NECLIME framework. We acknowledge the model support of the CLM community and the technical support from Juha Lento and Tommi Bergman in performing model experiments at the Center for Scientific Computing (CSC) in Espoo (Finland). The valuable comments from Mikael Fortelius and two anonymous reviewers are also highly appreciated.

## References

- Allen M, Jackson J, Walker R (2004) Late Cenozoic reorganization of the Arabia–Eurasia collision and the comparison of short-term and long-term deformation rates. *Tectonics* 23(2). doi:[10.1029/2003tc001530](https://doi.org/10.1029/2003tc001530)
- An ZS, Kutzbach JE, Prell WL, Porter SC (2001) Evolution of Asian monsoons and phased uplift of the Himalayan Tibetan plateau since Late Miocene times. *Nature* 411(6833):62–66
- An S-I, Park J-H, Kim B-M, Timmermann A, Jin F-F (2012) Impacts of ocean gateway and basin width on tertiary tropical climate variability in a prototype model. *Theor Appl Climatol* 107(1):155–164. doi:[10.1007/s00704-011-0469-x](https://doi.org/10.1007/s00704-011-0469-x)
- Ashfaq M, Shi Y, Tung WW, Trapp RJ, Gao XJ, Pal JS, Diffenbaugh NS (2009) Suppression of south Asian summer monsoon precipitation in the 21st century. *Geophys Res Lett* 36(1). doi:[10.1029/2008gl036500](https://doi.org/10.1029/2008gl036500)
- Barnett TP, Dumenil L, Schlese U, Roekner E (1988) The effect of Eurasian snow cover on global climate. *Science* 239(4839):504–507
- Barreiro M, Philander G, Pacanowski R, Fedorov A (2006) Simulations of warm tropical conditions with application to middle Pliocene atmospheres. *Clim Dyn* 26(4):349–365. doi:[10.1007/s00382-005-0086-4](https://doi.org/10.1007/s00382-005-0086-4)
- Beerling DJ, Royer DL (2011) Convergent Cenozoic CO<sub>2</sub> history. *Nat Geosci* 4(7):418–420. doi:[10.1038/Ngeo1186](https://doi.org/10.1038/Ngeo1186)
- Bradshaw CD, Lunt DJ, Flecker R, Salzmann U, Pound MJ, Haywood AM, Eronen JT (2012) The relative roles of CO<sub>2</sub> and palaeogeography in determining late Miocene climate: results from a terrestrial model-data comparison. *Clim Past* 8(4):1257–1285. doi:[10.5194/cp-8-1257-2012](https://doi.org/10.5194/cp-8-1257-2012)
- Brierley CM, Fedorov AV (2010) Relative importance of meridional and zonal sea surface temperature gradients for the onset of the ice ages and Pliocene–Pleistocene climate evolution. *Paleoceanography* 25(2):PA2214. doi:[10.1029/2009pa001809](https://doi.org/10.1029/2009pa001809)
- Chang CP, Harr P, Ju JH (2001) Possible roles of Atlantic circulations on the weakening Indian monsoon rainfall–ENSO relationship. *J Clim* 14(11):2376–2380
- Charreau J, Chen Y, Gilder S, Barrier L, Dominguez S, Augier R, Sen S, Avouac JP, Gallaud A, Graveleau F, Wang QC (2009) Neogene uplift of the Tian Shan mountains observed in the magnetic record of the Jingou River section (northwest China). *Tectonics* 28. doi:[10.1029/2007tc002137](https://doi.org/10.1029/2007tc002137)
- Clift PD, Hodges KV, Heslop D, Hannigan R, Van Long H, Calves G (2008) Correlation of Himalayan exhumation rates and Asian monsoon intensity. *Nat Geosci* 1(12):875–880. doi:[10.1038/ngeo351](https://doi.org/10.1038/ngeo351)
- Coleman M, Hodges K (1995) Evidence for Tibetan Plateau uplift before 14 Myr ago from a new minimum age for east–west extension. *Nature* 374(6517):49–52
- Collins LS, Coates AG, Berggren WA, Aubry MP, Zhang JJ (1996) The late Miocene Panama isthmian strait. *Geology* 24(8):687–690
- Collins M, An SI, Cai WJ, Ganachaud A, Guilyardi E, Jin FF, Jochum M, Lengaigne M, Power S, Timmermann A, Vecchi G, Wittenberg A (2010) The impact of global warming on the tropical Pacific Ocean and El Niño. *Nat Geosci* 3(6):391–397
- Cruz RV, Harasawa H, Lal M, Wu S, Anokhin Y, Punsalma B, Honda Y, Jafari M, Li C, Hsu Ninh N (2007) Asia climate change: impacts, adaptation and vulnerability. Contribution of Working Group II to the fourth assessment report of the intergovernmental panel on climate change. Cambridge University Press, Cambridge
- Dettman DL, Kohn MJ, Quade J, Ryerson FJ, Ojha TP, Hamidullah S (2001) Seasonal stable isotope evidence for a strong Asian monsoon throughout the past 10.7 my. *Geology* 29(1):31–34
- Ding QH, Wang B (2005) Circumglobal teleconnection in the Northern Hemisphere summer. *J Clim* 18(17):3483–3505
- Dobler A, Ahrens B (2010) Analysis of the Indian summer monsoon system in the regional climate model COSMO–CLM. *J Geophys Res* 115:D16101. doi:[10.1029/2009jd013497](https://doi.org/10.1029/2009jd013497)
- Dobler A, Ahrens B (2011) Four climate change scenarios for the Indian summer monsoon by the regional climate model COSMO–CLM. *J Geophys Res* 116:D24104. doi:[10.1029/2011jd016329](https://doi.org/10.1029/2011jd016329)
- Dong B, Sutton RT (2007) Enhancement of ENSO variability by a weakened Atlantic thermohaline circulation in a coupled GCM. *J Clim* 20(19):4920–4939
- Dupont-Nivet G, Krijgsman W, Langereis CG, Abels HA, Dai S, Fang X (2007) Tibetan plateau aridification linked to global cooling at the Eocene–Oligocene transition. *Nature* 445(7128):635–638. doi:[10.1038/nature05516](https://doi.org/10.1038/nature05516)
- Eronen JT, Ataabadia MM, Micheelsb A, Karne A, Bernor RL, Fortelius M (2009) Distribution history and climatic controls of the Late Miocene Pliocene chronofauna. *Proc Natl Acad Sci USA* 106(29):11867–11871. doi:[10.1073/pnas.0902598106](https://doi.org/10.1073/pnas.0902598106)
- Eronen JT, Puolamäki K, Liu L, Lintulaakso K, Damuth J, Janis C, Fortelius M (2010) Precipitation and large herbivorous mammals, part II: application to fossil data. *Evol Ecol Res* 12:235–248
- Eronen JT, Fortelius M, Micheels A, Portmann FT, Puolamäki K, Janis CM (2012) Neogene aridification of the Northern Hemisphere. *Geology* 40(9):823–826. doi:[10.1130/g33147.1](https://doi.org/10.1130/g33147.1)
- Fasullo J (2004) A stratified diagnosis of the Indian monsoon—Eurasian snow cover relationship. *J Clim* 17(5):1110–1122. doi:[10.1175/1520-0442\(2004\)017<1110:asdoti>2.0.co;2](https://doi.org/10.1175/1520-0442(2004)017<1110:asdoti>2.0.co;2)
- Fedorov AV, Brierley CM, Emanuel K (2010) Tropical cyclones and permanent El Niño in the early Pliocene epoch. *Nature* 463(7284):1066–1070
- Fu YH, Lu RY (2010) Simulated change in the interannual variability of South Asian summer monsoon in the 21st century. *Adv Atmos Sci* 27(5):992–1002. doi:[10.1007/s00376-009-9124-1](https://doi.org/10.1007/s00376-009-9124-1)
- Gadgil S (2003) The Indian monsoon and its variability. *Annu Rev Earth Planet Sci* 31:429–467. doi:[10.1146/annurev.earth.31.100901.141251](https://doi.org/10.1146/annurev.earth.31.100901.141251)



- Galeotti S, von der Heydt A, Huber M, Bice D, Dijkstra H, Jilbert T, Lanci L, Reichert GJ (2010) Evidence for active El Niño Southern oscillation variability in the Late Miocene greenhouse climate. *Geology* 38(5):419–422
- Ge J, Dai Y, Zhang Z, Zhao D, Li Q, Zhang Y, Yi L, Wu H, Oldfield F, Guo Z (2012) Major changes in East Asian climate in the mid-Pliocene: triggered by the uplift of the Tibetan Plateau or global cooling? *J Asian Earth Sci*. doi:10.1016/j.jseas.2012.10.009
- Goldner A, Huber M, Diffenbaugh N, Caballero R (2011) Implications of the permanent El Niño teleconnection “blueprint” for past global and North American hydroclimatology. *Clim Past* 7(3):723–743. doi:10.5194/cp-7-723-2011
- Goswami BN, Krishnamurthy V, Annamalai H (1999) A broad-scale circulation index for the interannual variability of the Indian summer monsoon. *Q J R Meteorol Soc* 125(554):611–633
- Guilyardi E (2006) El Niño-mean state-seasonal cycle interactions in a multi-model ensemble. *Clim Dyn* 26(4):329–348. doi:10.1007/s00382-005-0084-6
- Guilyardi E, Wittenberg A, Fedorov A, Collins M, Wang CZ, Capotondi A, van Oldenborgh GJ, Stockdale T (2009) Understanding El Niño in Ocean–atmosphere general circulation models progress and challenges. *Bull Am Meteorol Soc* 90(3):325–340. doi:10.1175/2008bams2387.1
- Harzhauser M, Piller WE (2007) Benchmark data of a changing sea—palaeogeography, palaeobiogeography and events in the Central Paratethys during the Miocene. *Palaeogeogr Palaeoclimatol Palaeoecol* 253(1–2):8–31
- Haywood AM, Valdes PJ, Peck VL (2007) A permanent El Niño-like state during the Pliocene? *Paleoceanography* 22(1). doi:10.1029/2006pa001323
- Haywood AM, Dowsett HJ, Valdes PJ, Lunt DJ, Francis JE, Sellwood BW (2009) Introduction. Pliocene climate, processes and problems. *Philos Trans R Soc A* 367(1886):3–17. doi:10.1098/rsta.2008.0205
- Herold N, Seton M, Muller RD, You Y, Huber M (2008) Middle Miocene tectonic boundary conditions for use in climate models. *Geochem Geophys Geosyst* 9:Q10009. doi:10.1029/2008GC002046
- Herold N, Huber M, Müller RD (2011) Modeling the Miocene climatic optimum. Part I: land and atmosphere. *J Clim* 24(24):6353–6372. doi:10.1175/2011jcli4035.1
- Hoorn C, Ohja T, Quade J (2000) Palynological evidence for vegetation development and climatic change in the Sub-Himalayan Zone (Neogene, Central Nepal). *Palaeogeogr Palaeoclimatol Palaeoecol* 163(3–4):133–161
- Huang YS, Clemens SC, Liu WG, Wang Y, Prell WL (2007) Large-scale hydrological change drove the late Miocene C<sub>4</sub> plant expansion in the Himalayan foreland and Arabian Peninsula. *Geology* 35(6):531–534. doi:10.1130/g23666a.1
- Huber M, Caballero R (2003) Eocene El Niño: evidence for robust tropical dynamics in the “hothouse”. *Science* 299(5608):877–881
- Huber M, Goldner A (2012) Eocene monsoons. *J Asian Earth Sci* 44:3–23. doi:10.1016/j.jseas.2011.09.014
- IPCC (2007) Climate change 2007: the physical science basis. Contribution of Working Group I to the fourth assessment report of the intergovernmental panel on climate change. Cambridge University Press, Cambridge
- Ivany LC, Brey T, Huber M, Buick DP, Schöne BR (2011) El Niño in the Eocene greenhouse recorded by fossil bivalves and wood from Antarctica. *Geophys Res Lett* 38(16):L16709. doi:10.1029/2011GL048635
- Jochum M, Fox-Kemper B, Molnar PH, Shields C (2009) Differences in the Indonesian seaway in a coupled climate model and their relevance to Pliocene climate and El Niño. *Paleoceanography* 24(1):PA1212. doi:10.1029/2008pa001678
- Ju JH, Slingo J (1995) The Asian summer monsoon and ENSO. *Q J R Meteorol Soc* 121(525):1133–1168
- Jungclaus JH, Keenlyside N, Botzet M, Haak H, Luo JJ, Latif M, Marotzke J, Mikolajewicz U, Roeckner E (2006) Ocean circulation and tropical variability in the coupled model ECHAM5/MPI-OM. *J Clim* 19(16):3952–3972
- Kalnay E, Kanamitsu M, Kistler R, Collins W, Deaven D, Gandin L, Iredell M, Saha S, White G, Woollen J, Zhu Y, Chelliah M, Ebisuzaki W, Higgins W, Janowiak J, Mo KC, Ropelewski C, Wang J, Leetmaa A, Reynolds R, Jenne R, Joseph D (1996) The NCEP/NCAR 40-year reanalysis project. *Bull Am Meteorol Soc* 77(3):437–471
- Kitoh A (2007) ENSO modulation by mountain uplift. *Clim Dyn* 28(7):781–796. doi:10.1007/s00382-006-0209-6
- Knorr G, Butzin M, Micheels A, Lohmann G (2011) A warm Miocene climate at low atmospheric CO<sub>2</sub> levels. *Geophys Res Lett* 38(20):L20701. doi:10.1029/2011gl048873
- Krapp M (2012) Middle Miocene climate evolution: the role of large-scale Ocean circulation and ocean gateways. Doctoral thesis, Max–Planck-Institut für Meteorologie, Hamburg
- Kripalani RH, Oh JH, Chaudhari HS (2007a) Response of the East Asian summer monsoon to doubled atmospheric CO<sub>2</sub>: coupled climate model simulations and projections under IPCC AR4. *Theor Appl Climatol* 87(1–4):1–28. doi:10.1007/s00704-006-0238-4
- Kripalani RH, Oh JH, Kulkarni A, Sabade SS, Chaudhari HS (2007b) South Asian summer monsoon precipitation variability: coupled climate model simulations and projections under IPCC AR4. *Theor Appl Climatol* 90(3–4):133–159. doi:10.1007/s00704-006-0282-0
- Kroon D, Steens T, Troelstra SR (1991) Onset of monsoonal related upwelling in the western Arabian Sea as revealed by planktonic foraminifers. *Proc Ocean Drill Program* 117:257–263
- Kurschner WM, Kvacek Z, Dilcher DL (2008) The impact of Miocene atmospheric carbon dioxide fluctuations on climate and the evolution of terrestrial ecosystems. *Proc Natl Acad Sci USA* 105(2):449–453. doi:10.1073/pnas.0708588105
- Kutzbach JE, Behling P (2004) Comparison of simulated changes of climate in Asia for two scenarios: early Miocene to present, and present to future enhanced greenhouse. *Glob Planet Chang* 41(3–4):157–165. doi:10.1016/j.gloplacha.2004.01.015
- Lacombe O, Mouthereau F, Kargar S, Meyer B (2006) Late Cenozoic and modern stress fields in the western Fars (Iran): implications for the tectonic and kinematic evolution of central Zagros. *Tectonics* 25(1):TC1003. doi:10.1029/2005TC001831
- Li JP, Wang JL (2003) A new North Atlantic oscillation index and its variability. *Adv Atmos Sci* 20(5):661–676. doi:10.1007/bf02915394
- Liu LP, Eronen JT, Fortelius M (2009) Significant mid-latitude aridity in the middle Miocene of East Asia. *Palaeogeogr Palaeoclimatol Palaeoecol* 279(3–4):201–206. doi:10.1016/j.palaeo.2009.05.014
- Liu-Zeng J, Tapponnier P, Gaudemer Y, Ding L (2008) Quantifying landscape differences across the Tibetan plateau: implications for topographic relief evolution. *J Geophys Res* 113:F04018. doi:10.1029/2007jf000897
- Lu RY, Chen W, Dong BW (2008) How does a weakened Atlantic thermohaline circulation lead to an intensification of the ENSO-south Asian summer monsoon interaction? *Geophys Res Lett* 35(8). doi:10.1029/2008gl033394
- Lunt DJ, Flecker R, Valdes PJ, Salzmann U, Gladstone R, Haywood AM (2008) A methodology for targeting palaeo proxy data acquisition: a case study for the terrestrial late Miocene. *Earth Planet Sci Lett* 271(1–4):53–62. doi:10.1016/j.epsl.2008.03.035
- Micheels A, Bruch AA, Uhl D, Utescher T, Mosbrugger V (2007) A Late Miocene climate model simulation with ECHAM4/ML and its quantitative validation with terrestrial proxy data. *Palaeogeogr*

- Palaeoclimatol Palaeoecol 253:251–270. doi:[10.1016/j.palaeo.2007.03.042](https://doi.org/10.1016/j.palaeo.2007.03.042)
- Micheels A, Bruch AA, Eronen J, Fortelius M, Harzhauser M, Utescher T, Mosbrugger V (2011) Analysis of heat transport mechanisms from a Late Miocene model experiment with a fully-coupled atmosphere–ocean general circulation model. *Palaeogeogr Palaeoclimatol Palaeoecol* 304(3–4):337–350
- Molnar P, Cane MA (2002) El Niño's tropical climate and teleconnections as a blueprint for pre-ice age climates. *Paleoceanography* 17(2):1021. doi:[10.1029/2001pa000663](https://doi.org/10.1029/2001pa000663)
- Molnar P, Boos WR, Battisti DS (2010) Orographic controls on climate and paleoclimate of Asia: thermal and mechanical roles for the Tibetan Plateau. *Annu Rev Earth Planet Sci* 38:77–102
- Muller WA, Roeckner E (2008) ENSO teleconnections in projections of future climate in ECHAM5/MPI-OM. *Clim Dyn* 31(5):533–549
- Paeth H, Hense A, Glowienka-Hense R, Voss S, Cubasch U (1999) The North Atlantic oscillation as an indicator for greenhouse-gas induced regional climate change. *Clim Dyn* 15(12):953–960. doi:[10.1007/s003820050324](https://doi.org/10.1007/s003820050324)
- Paeth H, Scholten A, Friederichs P, Hense A (2008) Uncertainties in climate change prediction: El Niño-Southern oscillation and monsoons. *Glob Planet Chang* 60(3–4):265–288. doi:[10.1016/j.gloplacha.2007.03.002](https://doi.org/10.1016/j.gloplacha.2007.03.002)
- Pagani M, Freeman KH, Arthur MA (1999) Late Miocene atmospheric CO<sub>2</sub> concentrations and the expansion of C<sub>4</sub> grasses. *Science* 285(5429):876–879. doi:[10.1126/science.285.5429.876](https://doi.org/10.1126/science.285.5429.876)
- Pagani M, Zachos JC, Freeman KH, Tipler B, Bohaty S (2005) Marked decline in atmospheric carbon dioxide concentrations during the Paleogene. *Science* 309(5734):600–603
- Parthasarathy B, Kumar KK, Kothawale DR (1992) Indian summer monsoon rainfall indices: 1871–1990. *Meteorol Mag* 121(1441):174–186
- Parthasarathy B, Munot AA, Kothawale DR (1994) All-India monthly and seasonal rainfall series—1871–1993. *Theor Appl Climatol* 49(4):217–224
- Pearson PN, Palmer MR (2000) Atmospheric carbon dioxide concentrations over the past 60 million years. *Nature* 406(6797):695–699
- Peings Y, Douville H (2010) Influence of the Eurasian snow cover on the Indian summer monsoon variability in observed climatologies and CMIP3 simulations. *Clim Dyn* 34(5):643–660. doi:[10.1007/s00382-009-0565-0](https://doi.org/10.1007/s00382-009-0565-0)
- Popov SV, Shcherba IG, Ilyina LB, Nevesskaya LA, Paramonova NP, Khondkarian SO, Magyar I (2006) Late Miocene to Pliocene palaeogeography of the Paratethys and its relation to the Mediterranean. *Palaeogeogr Palaeoclimatol Palaeoecol* 238(1–4):91–106. doi:[10.1016/j.palaeo.2006.03.020](https://doi.org/10.1016/j.palaeo.2006.03.020)
- Pound MJ, Haywood AM, Salzmann U, Riding JB, Lunt DJ, Hunter SJ (2011) A Tortonian (Late Miocene, 11.61–7.25 Ma) global vegetation reconstruction. *Palaeogeogr Palaeoclimatol Palaeoecol* 300(1–4):29–45. doi:[10.1016/j.palaeo.2010.11.029](https://doi.org/10.1016/j.palaeo.2010.11.029)
- Pound MJ, Haywood AM, Salzmann U, Riding JB (2012) Global vegetation dynamics and latitudinal temperature gradients during the Mid to Late Miocene (15.97–5.33 Ma). *Earth Sci Rev* 112(1–2):1–22. doi:[10.1016/j.earscirev.2012.02.005](https://doi.org/10.1016/j.earscirev.2012.02.005)
- Prell WL, Kutzbach JE (1992) Sensitivity of the Indian monsoon to forcing parameters and implications for its evolution. *Nature* 360(6405):647–652
- Quade J, Cerling TE, Bowman JR (1989) Development of Asian monsoon revealed by marked ecological shift during the Latest Miocene in Northern Pakistan. *Nature* 342(6246):163–166
- Robock A, Mu M, Vinnikov K, Robinson D (2003) Land surface conditions over Eurasia and Indian summer monsoon rainfall. *J Geophys Res* 108(D4):4131. doi:[10.1029/2002jd002286](https://doi.org/10.1029/2002jd002286)
- Rockel B, Geyer B (2008) The performance of the regional climate model CLM in different climate regions, based on the example of precipitation. *Meteorol Z* 17(4):487–498. doi:[10.1127/0941-2948/2008/0297](https://doi.org/10.1127/0941-2948/2008/0297)
- Rowley DB, Currie BS (2006) Palaeo-altimetry of the late Eocene to Miocene Lunpola basin, central Tibet. *Nature* 439(7077):677–681
- Rowley DB, Pierrehumbert RT, Currie BS (2001) A new approach to stable isotope-based paleoaltimetry: implications for paleoaltimetry and paleohypsometry of the High Himalaya since the Late Miocene. *Earth Planet Sci Lett* 188(1–2):253–268
- Saeed S, Müller W, Hagemann S, Jacob D (2011) Circumglobal wave train and the summer monsoon over northwestern India and Pakistan: the explicit role of the surface heat low. *Clim Dyn* 37(5–6):1045–1060. doi:[10.1007/s00382-010-0888-x](https://doi.org/10.1007/s00382-010-0888-x)
- Sanyal P, Sarkar A, Bhattacharya SK, Kumar R, Ghosh SK, Agrawal S (2010) Intensification of monsoon, microclimate and asynchronous C<sub>4</sub> appearance: isotopic evidence from the Indian Siwalik sediments. *Palaeogeogr Palaeoclimatol Palaeoecol* 296(1–2):165–173
- Schneck R, Micheels A, Mosbrugger V (2012) Climate impact of high northern vegetation: Late Miocene and present. *Int J Earth Sci* 101(1):323–338. doi:[10.1007/s00531-011-0652-4](https://doi.org/10.1007/s00531-011-0652-4)
- Scroton N, Bonham SG, Rickaby REM, Lawrence SHF, HERNANDEZ M, Haywood AM (2011) Persistent El Niño-Southern oscillation variation during the Pliocene Epoch. *Paleoceanography* 26(2):PA2215. doi:[10.1029/2010PA002097](https://doi.org/10.1029/2010PA002097)
- Shukla SP, Chandler MA, Jonas J, Sohl LE, Mankoff K, Dowsett H (2009) Impact of a permanent El Niño (El Padre) and Indian Ocean dipole in warm Pliocene climates. *Paleoceanography* 24(2):PA2221. doi:[10.1029/2008pa001682](https://doi.org/10.1029/2008pa001682)
- Smith TM, Reynolds RW, Peterson TC, Lawrimore J (2008) Improvements to NOAA's historical merged land-ocean surface temperature analysis (1880–2006). *J Clim* 21(10):2283–2296. doi:[10.1175/2007jcli2100.1](https://doi.org/10.1175/2007jcli2100.1)
- Spicer RA, Harris NBW, Widdowson M, Herman AB, Guo SX, Valdes PJ, Wolfe JA, Kelley SP (2003) Constant elevation of southern Tibet over the past 15 million years. *Nature* 421(6923):622–624
- Stappuhn A, Micheels A, Bruch AA, Uhl D, Utescher T, Mosbrugger V (2007) The sensitivity of ECHAM4/ML to a double CO<sub>2</sub> scenario for the Late Miocene and the comparison to terrestrial proxy data. *Glob Planet Chang* 57(3–4):189–212. doi:[10.1016/j.gloplacha.2006.09.003](https://doi.org/10.1016/j.gloplacha.2006.09.003)
- Sun XJ, Wang PX (2005) How old is the Asian monsoon system? Palaeobotanical records from China. *Palaeogeogr Palaeoclimatol Palaeoecol* 222(3–4):181–222
- Sun JM, Ye J, Wu WY, Ni XJ, Bi SD, Zhang ZQ, Liu WM, Meng J (2010) Late Oligocene–Miocene mid-latitude aridification and wind patterns in the Asian interior. *Geology* 38(6):515–518
- Syed F, Yoo J, Körnich H, Kucharski F (2012) Extratropical influences on the inter-annual variability of South-Asian monsoon. *Clim Dyn* 38(7):1661–1674. doi:[10.1007/s00382-011-1059-4](https://doi.org/10.1007/s00382-011-1059-4)
- Tang H, Micheels A, Eronen J, Fortelius M (2011) Regional climate model experiments to investigate the Asian monsoon in the Late Miocene. *Clim Past* 7(3):847–868
- Tang H, Micheels A, Eronen J, Ahrens B, Fortelius M (2012) Asynchronous responses of East Asian and Indian summer monsoons to mountain uplift shown by regional climate modelling experiments. *Clim Dyn* 1–19. doi:[10.1007/s00382-012-1603-x](https://doi.org/10.1007/s00382-012-1603-x)
- Tong JA, You Y, Müller RD, Seton M (2009) Climate model sensitivity to atmospheric CO<sub>2</sub> concentrations for the middle Miocene. *Glob Planet Chang* 67(3–4):129–140. doi:[10.1016/j.gloplacha.2009.02.001](https://doi.org/10.1016/j.gloplacha.2009.02.001)
- Turner AG, Slingo JM (2011) Using idealized snow forcing to test teleconnections with the Indian summer monsoon in the Hadley

- Centre GCM. *Clim Dyn* 36(9–10):1717–1735. doi:[10.1007/s00382-010-0805-3](https://doi.org/10.1007/s00382-010-0805-3)
- Utescher T, Bruch AA, Micheels A, Mosbrugger V, Popova S (2011) Cenozoic climate gradients in Eurasia—a palaeo-perspective on future climate change? *Palaeogeogr Palaeoclimatol Palaeoecol* 304(3–4):351–358. doi:[10.1016/j.palaeo.2010.09.031](https://doi.org/10.1016/j.palaeo.2010.09.031)
- Vernekar AD, Zhou J, Shukla J (1995) The effect of Eurasian snow cover on the Indian monsoon. *J Clim* 8(2):248–266
- Vizcaíno M, Rupper S, Chiang JCH (2010) Permanent El Niño and the onset of Northern Hemisphere glaciations: mechanism and comparison with other hypotheses. *Paleoceanography* 25(2):PA2205. doi:[10.1029/2009pa001733](https://doi.org/10.1029/2009pa001733)
- von der Heydt A, Dijkstra H (2011) The impact of ocean gateways on ENSO variability in the Miocene. *Geol Soc Lond Spec Publ* 355:305–318. doi:[10.1144/SP355.15](https://doi.org/10.1144/SP355.15)
- Wang B, Wu RG, Lau KM (2001) Interannual variability of the Asian summer monsoon: contrasts between the Indian and the western North Pacific–east Asian monsoons. *J Clim* 14(20):4073–4090
- Wang PX, Clemens S, Beaufort L, Braconnot P, Ganssen G, Jian ZM, Kershaw P, Sarnthein M (2005) Evolution and variability of the Asian monsoon system: state of the art and outstanding issues. *Quat Sci Rev* 24(5–6):595–629
- Wang Y, Wang XM, Xu YF, Zhang CF, Li Q, Tseng ZJ, Takeuchi G, Deng T (2008) Stable isotopes in fossil mammals, fish and shells from Kunlun Pass Basin, Tibetan Plateau: paleo-climatic and paleo-elevation implications. *Earth Planet Sci Lett* 270(1–2): 73–85. doi:[10.1016/j.epsl.2008.03.006](https://doi.org/10.1016/j.epsl.2008.03.006)
- Wara MW, Ravelo AC, Delaney ML (2005) Permanent El Niño-like conditions during the Pliocene warm period. *Science* 309(5735): 758–761. doi:[10.1126/science.1112596](https://doi.org/10.1126/science.1112596)
- Watanabe T, Suzuki A, Minobe S, Kawashima T, Kameo K, Minoshima K, Aguilar YM, Wani R, Kawahata H, Sowa K, Nagai T, Kase T (2011) Permanent El Niño during the Pliocene warm period not supported by coral evidence. *Nature* 471(7337): 209–211. doi:[10.1038/Nature09777](https://doi.org/10.1038/Nature09777)
- Webster PJ, Magana VO, Palmer TN, Shukla J, Tomas RA, Yanai M, Yasunari T (1998) Monsoons: processes, predictability, and the prospects for prediction. *J Geophys Res* 103(C7):14451–14510
- Wu AM, Ni YQ (1997) The influence of Tibetan plateau on the interannual variability of Asian monsoon. *Adv Atmos Sci* 14(4):491–504. doi:[10.1007/s00376-997-0067-0](https://doi.org/10.1007/s00376-997-0067-0)
- Yang S, Lau KM (2006) Interannual variability of the Asian monsoon. In: Wang B (ed) *The Asian monsoon*. Springer, Berlin, pp 259–293
- Ye HC, Bao ZH (2001) Lagged teleconnections between snow depth in northern Eurasia, rainfall in Southeast Asia and sea-surface temperatures over the tropical Pacific Ocean. *Int J Climatol* 21(13):1607–1621
- Yeh SW, Kug JS, Dewitte B, Kwon MH, Kirtman BP, Jin FF (2009) El Niño in a changing climate. *Nature* 461(7263):511–514. doi:[10.1038/Nature08316](https://doi.org/10.1038/Nature08316)
- Yin A (2010) Cenozoic tectonic evolution of Asia: a preliminary synthesis. *Tectonophysics* 488(1–4):293–325
- Zachos J, Pagani M, Sloan L, Thomas E, Billups K (2001) Trends, rhythms, and aberrations in global climate 65 Ma to present. *Science* 292(5517):686–693
- Zhang Z, Flatøy F, Wang H, Bethke I, Bentsen M, Guo Z (2012) Early Eocene Asian climate dominated by desert and steppe with limited monsoons. *J Asian Earth Sci* 44:24–35. doi:[10.1016/j.jseas.2011.05.013](https://doi.org/10.1016/j.jseas.2011.05.013)
- Zheng HB, Powell CM, An ZS, Zhou J, Dong GR (2000) Pliocene uplift of the northern Tibetan Plateau. *Geology* 28(8):715–718